Chapter 2

The Mini AGN at the Center of the Elliptical Galaxy NGC 4552 with HST[1]

Abstract

The complex phenomenology shown by the UV-bright, variable spike first detected with the Hubble Space Telescope (HST) at the center of the otherwise normal galaxy NGC 4552 is further investigated with both HST imaging (FOC) and spectroscopy (FOS). HST/FOC images taken in 1991, 1993, and 1996 in the near UV have been analyzed in a homogeneous fashion, showing that the central spike has brightened by a factor ~ 4.5 between 1991 and 1993, and has decreased its luminosity by a factor ~ 2.0 between 1993 and 1996. FOS spectroscopy extending from the near UV to the red side of the optical spectrum reveals a strong UV continuum over the spectrum of the underlying galaxy, along with several emission lines in both the UV and the optical ranges. In spite of the low luminosity of the UV continuum of the spike ($\sim 3\times10^5 L_\odot$), the spike is definitely placed among AGNs by current diagnostics based on the emission line intensity ratios, being just on the borderline between Seyferts and LINERs. Line profiles are very broad, and both permitted *and* forbidden lines are best modelled with a combination of broad and narrow components, with FWHM of ~ 3000 km s^{-1} and ~ 700 km s^{-1}, respectively. This evidence argues for the variable central spike being produced by a modest accretion event onto a central massive black hole (BH), with the accreted material having possibly being stripped from a a star in a close fly by with the BH. The 1996 broad Hα luminosity of this mini-AGN is $\sim 5.6\times10^{37}$ erg s^{-1}, about a factor of two less than that of the nucleus of NGC 4395, heretofore considered to be the faintest known AGN. Combining all observational constraints, we estimate the mass of the BH at the center of NGC 4552 to be in the range between 3×10^8 and $2\times10^9 L_\odot$. The relevance for the demography of BHs in galaxies of the high (HST) resolution imaging and spectroscopy capable of revealing an extremely low level AGN activity in normal galaxies is briefly discussed.

[1]Cappellari, M., Renzini, A., Greggio, L., di Serego Alighieri, S., Buson, L. M., Burstein, D. & Bertola, F. 1999, ApJ, 519, 117

2.1 Introduction

With the intent of studying the stellar populations of early-type galaxies, in 1993 we obtained with the Faint Object Camera (FOC) on the Hubble Space Telescope (HST) images in several ultraviolet bands of the central regions of the elliptical galaxies NGC 1399 and NGC 4552 and of the bulge of the Sb galaxy NGC 2681. A point-like source – that we term *spike* for short – was evident at the center of both NGC 4552 and NGC 2681, with their photometric profile being indistinguishable from the PSF of the aberrated, pre-COSTAR HST (Bertola et al. 1995).

By comparison with another FOC image of NGC 4552 taken in 1991 (Crane et al. 1993), we soon realized that this spike had increased its luminosity in the U band (F342W) by a factor $\sim 7 \pm 1.5$ between the two epochs, reaching $\sim 10^6 \mathrm{L}_\odot$ (Renzini et al. 1995, hereafter Paper I). A second point-like source is also present in the 1991 image, $\sim 0\farcs14$ from the central spike and with nearly the same luminosity. While both sources were detected at the $\sim 4\sigma$ level in the 1991 image, the offcenter source was not detectable in the 1993 image at the $\sim 2.5\sigma$ level.

In Paper I we discussed several possible interpretations for the occurrence of such an ultraviolet *flare* at the center of NGC 4552, favoring an accretion event onto a central massive black hole (BH). The accreted material could have been tidally stripped from a star in a close fly-by with the BH, though alternative ways of feeding the BH were also considered. If the flaring spike was due to accretion onto a BH, its spectrum should show prominent, rotationally broadened emission lines, typical of an accretion disk (Renzini 1995). To check this expectation we then obtained further HST observations, both for spectroscopy with the Faint Object Spectrograph (FOS), and for imaging with FOC to follow the subsequent photometric evolution of the two sources. Indeed, with the superior performance of the post-COSTAR HST/FOC one could check whether any sign remained of the offcenter spike that was present only in the 1991 F342W image, and for which we had no obvious interpretation to offer (Paper I; Renzini 1995). The HST observations with both FOC and FOS were done on May 23, 1996, and the results are reported in this Chapter. These observations confirm the variability of the central source, the disappearance of the offcenter one, and lend conclusive support to the BH accretion interpretation of the event: indeed, very broad emission lines (FWHM $\simeq 3000$ km s^{-1}, for both permitted *and* forbidden lines!) characterize the spectrum of the variable nucleus of NGC 4552, and we argue that this object is likely to be the least luminous AGN so far discovered.

In terms of its physical properties, NGC 4552 (M89) is a rather typical giant elliptical galaxy in the Virgo cluster, having an absolute B magnitude of M_{B}=-20.2 (adopting a distance of 15.3 Mpc, cf. Faber et al. 1997), Its physical properties fit well the fundamental plane (Bender, Burstein & Faber 1992) as well as the $\mathrm{Mg}_2 - \sigma$ relation (Mg_2=0.343 mag, σ = 275 km s^{-1}; Davies et al. 1987; Bender, Burstein & Faber 1993). Even its far-UV properties are typical of gE galaxies of its Mg_2 strength (Burstein et al. 1988; Brown et al. 1995, 1997).

Hα emission extends from the center of NGC 4552 out to ~ 2.5 kpc (Trinchieri & di Serego Alighieri 1991; Macchetto et al. 1996), likely the result of a recent accretion of a small gas rich satellite, a rather common finding among giant ellipticals. Possibly related to this event are the inner dust patches first recognized by van Dokkum & Franx (1995) on early WFPC images, while the presence of a circumnuclear, dusty ring-like structure ($0\farcs2$ in diameter) encircling the central bright spike has been reported by Carollo et al. (1997a; cf. Section 2.4.5

of the present Chapter). This structure is virtually identical to a feature seen at the center of NGC 4261 (Jaffe et al. 1996). Yet, ground based spectroscopy with $2'' \times 4''$ apertures of the center of NGC 4552 reveals a spectrum dominated by broad absorption lines typical of the old stellar populations of ellipticals, and no obvious signs of nuclear activity (Davies et al. 1987; Ho, Filippenko, & Sargent 1995).

In X-ray properties, NGC 4552 has an unresolved "hard" X-ray source and a more diffuse, "soft" (i.e. thermal) X-ray source of comparable luminosity ($L_X \sim 10^{40.5}$ erg s^{-1}), as reported by Schlegel et al. (1998). This is well in the range of X-ray luminosities of ellipticals of similar optical luminosity (see e.g. Pellegrini 1994), with the emission being probably dominated by the hot interstellar medium. NGC 4552 also hosts a weak, compact radiosource that is variable on a time scale of several years (Jenkins 1982; Wrobel 1991). Therefore, several hints of BH-related nuclear activity have existed before our detection of the time-variable spike. Yet, NGC 1399 is a much stronger radiosource (Bolton, Wright, & Savage 1979), but our 1993 FOC images reveal no central spike.

As argued in Paper I, the UV high resolution imaging of the central regions of galactic spheroids – that currently can only be done with HST – can offer an attractive way of recognizing the presence of a massive BH. The traditional way of revealing the presence of central BHs in otherwise 'normal' galaxies is to resort to the kinematical behavior of stars and gas in their central regions, as very high velocities of *bound* matter within a tiny volume of the galaxy is the unmistakable signature of a massive compact object. As a consequence, evidence for central BHs in normal or weakly active galaxies has been extensively sought by means of stellar dynamics diagnostics (Kormendy & Richstone 1995; Bender et al. 1996; van der Marel et al. 1997; Kormendy et al. 1997; and references therein). The existence of a massive dark object (MDO, an euphemism for BH) at the center of *virtually all* elliptical and spiral bulges with a mass $M_\bullet \simeq (0.002 - 0.006) \times M_{\rm spheroid}$ is proposed by Kormendy & Richstone (1995) and Faber et al. (1997) (see Ho 1998 for a recent review). Dynamical modelling of a sample of 36 nearby galaxies appear to require the presence of a central MDO in at least 30 of them, with $M_\bullet \simeq 0.005 \times M_{\rm spheroid}$ (Magorrian et al. 1998). On this basis, we would expect the center of NGC 4552 to house a BH of mass 10^8 to 10^9 $M_\odot$.

Gas dynamics diagnostics has also been used, including studies of the optical emission lines originating in material orbiting the putative BH, with classical examples being the nuclear disk in in M87 (Ford et al. 1994), the spectacular H_2O megamaser at the center of NGC 4258 (Miyoshi et al. 1995), and the time-varying profile of the Hα emission at the center of the LINER galaxy NGC 1097 (Eracleous et al. 1995).

Besides the 1991 and 1993 FOC data and our May 1996 HST FOC and FOS data in this Chapter we also use data retrieved from the STScI archive, namely the January 1997 FOS spectra and WFPC2 images of Faber et al. (1997). The photometric evolution of the spike as seen in FOC images is presented in Section 2. In Section 3 the FOS spectroscopic observations are analyzed in detail. In Section 4 we discuss several implications of our findings. In particular, we compare the active nucleus in NGC 4552 to the previously known faintest AGN, i.e., NGC 4395 (Filippenko, Ho, & Sargent 1993), we speculate as to why the active nucleus is so faint, and why the 1991 offcenter spike has virtually disappeared. We then try to set constraints on the mass of the central BH, we compare the central spike in NGC 4552 to those seen in other nearby galaxies, and finally we discuss how the NGC 4552 phenomenon can be used to diagnose the presence of a central massive BH in other galaxies. Our conclusions are summarized in Section 5, while in the Appendix we give the technical details of our analysis of HST data.

Table 2.1: FOC f/96 Observation Log.

COSTAR	Observing Mode	Filter	Date	Exp. (s)
No	512×512	F342W	19 Jul 1991	1196
No	512×512	F502M	19 Jul 1991	896
No	512z×1024	F175W	28 Nov 1993	2453[a]
No	512z×1024	F220W	28 Nov 1993	1377
No	512z×1024	F275W	28 Nov 1993	717
No	512z×1024	F342W	28 Nov 1993	597
Yes	512×512	F175W	23 May 1996	1287
Yes	512×512	F275W	23 May 1996	384
Yes	512×512	F342W	23 May 1996	296

[a] Sum of two equal exposures

2.2 FOC Imaging

2.2.1 Observations

Pre-COSTAR FOC observations of NGC 4552 include a F342W and a F502M frame obtained on July 19, 1991 (Crane et al. 1993), and our own subsequent images obtained on November 28, 1993 in four adjacent UV passbands (F175W, F220W, F275W, F342W). The 1991 FOC/96 image was recorded in the 512×512 unzoomed mode yielding a field of view (FoV) of $11''\times11''$, whereas the zoomed 512×1024 mode (with a $22''\times22''$ FoV) was adopted for the 1993 observations. We then observed NGC 4552 for a third time on May 23, 1996 in the 512×512 unzoomed mode ($7''\times7''$ COSTAR-Corrected FoV) with the three UV filters (F175W, F275W and F342W). A summary of the instrumental configurations and exposure times is given in Table 2.1. The FOC observations have been calibrated using the standard STScI pipeline software. The most recent calibration files have been used when dearchiving and recalibrating the older data from the HST Archive.

2.2.2 Position of the Flare

The location of the central and offcenter spikes with respect to the photometric center of the galaxy is determined using the ELLIPSE task in IRAF/STSDAS over the F342W images obtained in 1991, 1993 and 1996. The result is shown in Figure 2.1 with superimposed a contour plot of the 1991, 1993 and 1996 images (3 pixel boxcar smoothed) of the very central region. Here the "X" denotes the position of the center of the $1''$ semimajor axis elliptical annulus. Note that the contour levels do not correspond to the same surface brightness on the different images, since they are only intended to display the position and structure of the spikes. The elliptical shape of the spike in the 1993 image is due to the zoomed mode of the original FOC image (see Table 2.1), while the smaller size of the spike in the 1996 image is an effect of the deployment of the COSTAR corrective optics.

The three plots have the same scale and orientation: north is up and east at the left. It can be seen that in 1991 the center of the galaxy coincides with one of the two point-sources seen in that image (cf. Paper I), while in the 1993 and 1996 images it coincides within $\sim 0\farcs02$ with the sole spike seen. This coincidence between the center of the galaxy and the spike has also

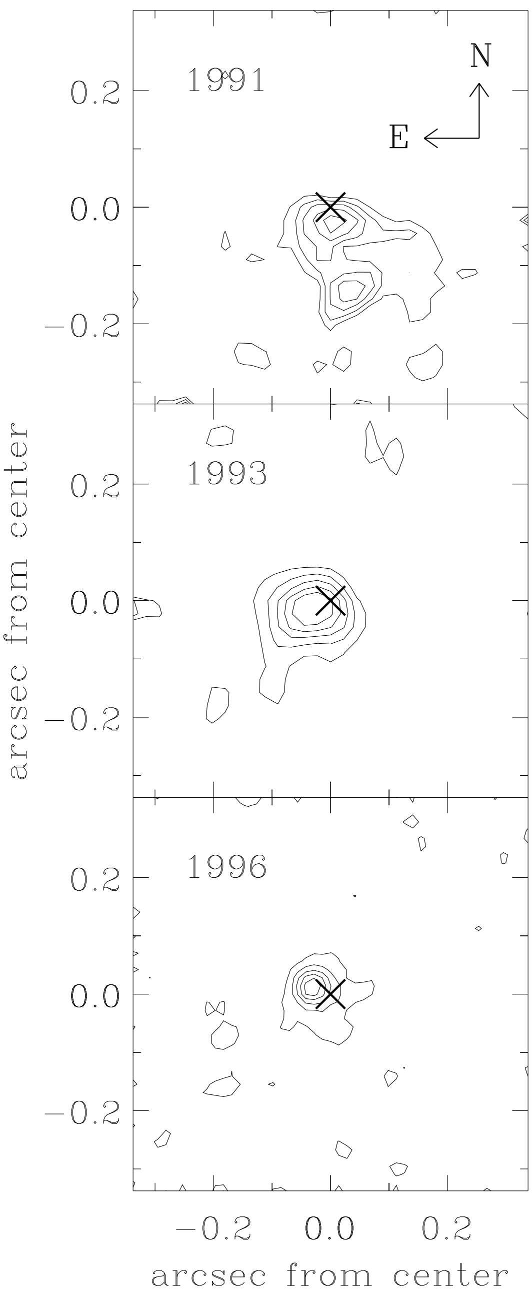

Figure 2.1: Contour plots of the very central region of NGC 4552 as recorded by FOC in the F342W waveband (FoV=$0''.6 \times 0''.6$). North is up and East to the left. Top, middle and bottom panel correspond to the 1991, 1993 and 1996 observations, respectively. The cross represents the photometric center of the galaxy as obtained by fitting to the light distribution of the galaxy an elliptical annulus with semi-major axis $a = 1''$ and width $\Delta a = 1''$. At all the three epochs the position of the spike coincides with the center of the galaxy within the errors ($\sim 0''.03$).

been verified on the images obtained with the other UV filters, although with lower accuracy, due to the lower S/N. We note that while the formal errors given by ELLIPSE on the galaxy center position are negligible, other factors, such as the accuracy of FOC flat-fielding and geometric corrections play a role in the determination of the center, so the small offset of the central spike with respect to the galaxy photometric center is not significant. On the other hand, the relative offset of the two point sources in the 1991 image is significant and reliably determined.

2.2.3 Photometric Modeling

To measure the luminosity of the central spikes one has to model the underlying surface brightness distribution of the galaxy. For this purpose we adopt the convenient parametrization now known as the "nuker" law (Lauer et al. 1995):

$$I(r) = I_{\rm b}\, 2^{\frac{\beta-\gamma}{\alpha}} \left(\frac{r}{r_{\rm b}}\right)^{-\gamma} \left[1+\left(\frac{r}{r_{\rm b}}\right)^{\alpha}\right]^{-\frac{\beta-\gamma}{\alpha}}, \tag{2.1}$$

where γ measures the steepness of the inner profile ($I(r) \propto r^{-\gamma}$ for $r \ll r_{\rm b}$), β is the steepness of the outer profile ($I(r) \propto r^{-\beta}$ for $r \gg r_{\rm b}$), α is related to the sharpness of the transition and $I_{\rm b}$ is a scale factor. To this profile we will add the contribution of an unresolved central point source (c_s), that represents the predicted flux of the *spike*. This kind of feature is present in a fair number ($\sim$25%) of the early-type galaxies modeled with a nuker law (Lauer et al. 1995, Carollo et al. 1997a,b). The derived parameters for each of the FOC epochs are given in Table 2.2.

The comparison of the FOC images obtained at the three epochs is complicated by two factors. First, each FOC image was obtained under different conditions: The 1991 image is pre-COSTAR, FOC-standard; the 1993 image is pre-COSTAR, FOC-zoomed, while the 1996 image is post-COSTAR, FOC-standard. Second, the 1993 images exceed the linearity limit of the FOC in some of the filters. As such, we have re-calibrated all the images in a self-consistent manner, including all required correction factors for PSF and sensitivity differences (zoom/non-zoomed modes and COSTAR) and nonlinearity effects.

In so doing, we are aided by the fact that the intrinsic luminosity profile of the galaxy in a given FOC filter has to be the same for all epochs. In contrast, we permit the luminosity of the spike to vary. Owing to the smaller field size of the post-COSTAR 1996 image, only the shape of the inner galaxy luminosity profile (i.e., the α, γ and $r_{\rm b}$ parameters) can be measured from the 1996 non-aberrated (linear) images. The slope of the outer luminosity profile (β) is better be measured from the 1993 images, which cover the largest field of view and from which the dark rate can be reliably determined within the shade of the coronographic fingers. In this way, for each FOC filter a unique two-dimensional luminosity distribution for NGC 4552 is obtained (as described by the parameters α, β, γ and $r_{\rm b}$. A two-dimensional model is required in order to apply the PSF-related corrections to the data.) We confirm that, when convolved in the appropriate manner for each FOC instrumental configuration, the galaxy luminosity profile accurately reproduces the observed profiles. What can, and does differ for each passband and epoch is the scale factor $I_{\rm b}$ and the excess counts $c_{\rm s}$ from the central spike (plus the second, off-center spike in the 1991 image). In practice, an iterative procedure was used to derive the galaxy and spike parameters, in the following manner:

Table 2.2: Fitted Parameters in Equation 2.1 obtained from the Photometric Modeling.

Filter	Date	α	β	γ	r_b	I_b	c_s
(1)	(2)	(3)	(4)	(5)	(6)	(7)	(8)
F502M	1991	2.89±0.34	1.020±0.034	0.00±0.03	0.507±0.022	140.1±4.0	1100±110
F342W	1991	3.51±0.81	1.016±0.061	0.00±0.03	0.514±0.037	134.86±0.70	1600±200
"	1993	"	"	"	"	85.60±0.89	4530±290
"	1996	"	"	"	"	9.39±0.44	589±31
F275W	1993	4.06±0.90	1.137±0.055	0.00±0.03	0.511±0.030	14.82±0.15	1870±110
"	1996	"	"	"	"	1.866±0.082	268±12
F220W	1993	"	1.35±0.19[a]	"	"	11.08±0.14	1165±84
F175W	1993	17±10	1.062±0.050	0.00±0.03	0.517±0.029	14.32±0.09	919±47
"	1996	"	"	"	"	1.640±0.089	142±11

[a] In the FOC F220W the S/N is low and the Nuker-law parameters can not be reliably determined: they have been imposed to be equal to those obtained for the F275W frames. On the other hand the outer profile appears significantly different from that of the other images, even taking into account the large error in the background subtraction: for this reason it has been independently measured.

Notes—Col. (1): FOC filter used in the observation; Col. (2): Date the observation was taken; Col. (3): The α Nuker-law parameter measures the sharpness of the break between the inner and the outer power-law profiles; Col. (4): The β parameter is the stepness of the outer profile ($I(r) \propto r^{-\beta}$ for $r \gg r_{\rm b}$); Col. (5): The γ parameter is the stepness of the inner profile ($I(r) \propto r^{-\gamma}$ for $r \ll r_{\rm b}$); Col. (6): r_b is the radius of the break, measured in arcsec; Col. (7): I_b is a scaling factor of the profile and indicates the surface brightness at $r = r_b$ in raw units (counts pixel^{-1}); Col. (8): c_s are the raw *total* counts of the spike. See text for details of how they have been measured. A " in this table means that this parameter has been held fixed at the value determined in above line, and it has not been fitted. See text for details.

1. A dark rate of 7×10^{-4} counts s^{-1} (Nota et al. 1996) is initially assumed and subtracted from the 1996 image. Since this is not the true background, this assumption will affect the determination of the outer Nuker law parameter β.

2. The initially background–subtracted image is then iteratively proceed through the following four steps (a—d) to provide a best-fit estimate of the Nuker-law parameters α, γ and $r_{\rm b}$. A Nelder-Mead Simplex algorithm is used for the first iterations, when the parameters are still far from the exact solution, while a Levenberg-Marquardt algorithm is used when the solution is approached to accelerate convergence and to estimate the errors (see Press et al. 1992). Since the ellipticity measured from our images is very small ($\varepsilon \lesssim 0.03$) and the position angle can not be reliably determined, $\varepsilon \equiv 0$ was set for all models.

   (a) A two dimensional synthetic model is made of the galaxy surface brightness distribution with a photometric profile described by Equation (2.1).

   (b) A certain number of counts c_s is added to the central pixel of this model to simulate the point-like central spike.

   (c) This synthetic image is then convolved with the appropriate PSF taken from the STScI library, and the effects of nonlinearity are included (described in Appendix 2.6.1).

   (d) The photometric profile of the *simulated* image of the galaxy is fit, on a log-log scale, to the photometric profile of the *observed* image by minimizing χ^2, and an improved full set of Nuker law and spike parameters is determined.

3. After the "inner" Nuker law parameters α, γ and $r_{\rm b}$ are determined from the previous step, the "outer" parameter β, the scale factor $I_{\rm b}$ and the counts from the spike c_s are iteratively fit to the 1993 image, following the procedure defined in Steps 2a–2d.

4. The value of β determined from the 1993 image is then used to iteratively constrain the dark count rate of the 1996 image, by requiring this image to yield the same value of β. During this step all other Nuker law parameters are kept fixed as determined by Step 2.

5. The resulting full set of parameters (α, γ, $r_{\rm b}$ and β) as determined from Steps 2–4 are then used as input and the process is begun again at Step 2 until convergence is reached for all parameters, including the spike count-rate, for the 1993 and 1996 FOC images.

The result of this iterative procedure is the determination of the Nuker parameters for all images of NGC 4552 in the three filters F175W, F275W, and F342W, plus the spike counts in the same bands for both the 1993 and 1996 images. The counts for the central spike in the F342W image of 1991 are then estimated (together with the scaling factor) as a free parameter of a fit whose Nuker law parameters are now forced to the values determined for both the 1993 and 1996 images. The counts of the off-center spike detected in our 1991 image is then separately determined by direct PSF-fitting.

For two filters, only one observation is available — F502W in 1991 and F220W in 1993 — so the above iterative procedure is not appliable. For the F220W image we have *assumed* that the parameters α, γ and r_b of the "Nuker" law are the same as for the F275W image and we only apply Step 3 of the sequence enumerated above. In the case of the F502M image, the contribution of the spike is negligible relative the galaxy luminosity profile itself, so we have fit all of the parameters using Steps 2a–2d.

2.2.4 Results

The results of the Nuker law plus central spike fits are shown in Figure 2.2 for all FOC images taken from 1991 to 1996, nine in all. Note that the fits have been restricted within $r < 3''$ from the center in order to better reproduce the nuclear profile and to reduce the sensitivity to dark subtraction errors. We have used the STScI magnitude system, defined by the relation

$$m_{\rm HST}^{\rm j} = -21.1 - 2.5\ \log \frac{\text{counts } U_{\rm j}}{T_{\rm j}} \tag{2.2}$$

where $U_{\rm j}$ is the filter inverse sensitivity and $T_{\rm j}$ is the exposure time. Determination of the inverse sensitivities is discussed below (Sec. 2.4.1). Note however that the definition of our photometric system is actually quite arbitrary, as the red leak of the UV filters can be significant and hard to predict for the red spectral energy distribution (SED) of the galaxy.

The numerical values of the parameters determined with these models are presented in Table 2.2. The 1–σ formal errors of the fit parameters are computed from the covariance matrix, so they follow from the shape of the χ^2 surface near its minimum. The parameters I_b and c_s in column (7) and (8) are given in units of raw counts, as it is in this form they will be discussed later.

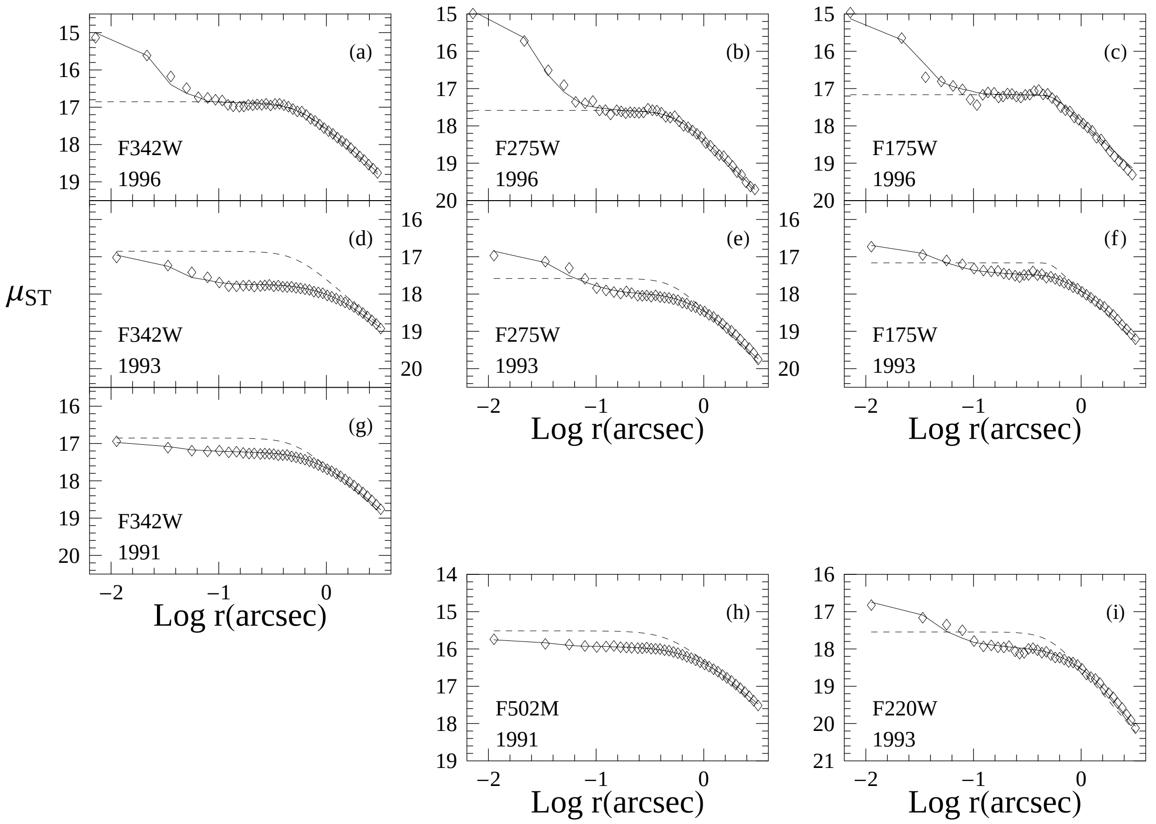

Figure 2.2: Modeling of the inner surface brightness profiles (HST magnitudes) of NGC 4552 vs. $\log r$ in different FOC wavebands. Diamonds represent the observed profile, the dashed line represents a model of the true galaxy profile and finally the solid line shows the above model after adding a point-like central source and then applying all the known instrumental effects of that specific observation (see text for details). Note that, within a specific waveband, the underlying (spike-free) galaxy model has been constrained to be the same at all epochs.

Table 2.3: Variation of the Spike and Relative Calibration of the Frames.

	Spike Variation		Sensitivity Variation	
Filter	f_{93}/f_{91}	f_{93}/f_{96}	U_{93}^{-1}/U_{91}^{-1}	U_{93}^{-1}/U_{96}^{-1}
F175W	⋯	1.8±0.2	⋯	1.86±0.10
F275W	⋯	2.2±0.2	⋯	1.73±0.08
F342W	4.5±0.6	2.1±0.2	1.27±0.02	1.84±0.09

Calibration of the Frames

The ratio $U_{\rm j}^{-1}/U_{\rm k}^{-1}$ of the sensitivity of two different frames obtained with the same filter is given by the following relation

$$\frac{U_{\rm j}^{-1}}{U_{\rm k}^{-1}} = \frac{I_{\rm b}^{\rm j}\ T_{\rm k}\ {\rm scale}_{\rm k}^2}{I_{\rm b}^{\rm k}\ T_{\rm j}\ {\rm scale}_{\rm j}^2} \tag{2.3}$$

where $I_{\rm b}^{\rm k}$ is the scaling factor (Table 2.2), $T_{\rm k}$ is the corresponding exposure time (Table 2.1), ${\rm scale}_{\rm k} = 0.02250$ arcsec pixel^{-1} for the pre-COSTAR observations (1991 and 1993) and ${\rm scale}_{\rm k} = 0.01435$ arcsec pixel^{-1} for the post-COSTAR ones (1996) (Nota et al. 1996).

In Table 2.3 we have computed the sensitivity ratios [Eq. (2.3)] between the different observing modes by taking the ratios of the galaxy model fluxes determined from the model fits (Sec. 2.3). The ratio of the 1993 galaxy model to the 1991 galaxy model depends on the sensitivity difference between the 512×1024 zoomed mode (1993) relative to the 512×512 standard mode (1991). The value of 1.27 ± 0.02 we derive from this comparison is very close to the 1.25 ± 0.05 factor tabulated in the latest FOC manual. This comparison makes us confident that our calibration method is reliable and accurate.

Although the 1991 and 1996 FOC frames are taken in the same observing mode (512×512 mode), we have to take into account the net decrease in sensitivity in the 1996 frame owing to two additional COSTAR reflections. In addition we also have to take into account any possible sensitivity degradation over this five year period. While the 1.45±0.07 decrease (1991 to 1996) we measure is bigger than the 1.23 value we get using the SYNPHOT package within IRAF/STSDAS, this difference is understandable in the following way: Our method separately accounts for sensitivity variations of the FOC from those relating to the different PSFs among these images. In contrast SYNPHOT estimates are based on aperture photometry of standard stars, which by its very nature combines PSF-related effects and sensitivity-related effects together into one correction. As a result we would expect our estimate of sensitivity decrease (1991 to 1996) to be larger than that obtained using SYNPHOT, which is what we observe.

Our estimates of sensitivity variations among the different FOC modes are conservative in the sense of minimizing the luminosity variation of the spike from 1993 to 1996. If we used the SYNPHOT estimates of sensitivity variation we would obtain a larger variation of the spike luminosity. To convert our relative fluxes to physical units, we *adopt* the STScI absolute calibration of the COSTAR corrected images (as given by SYNPHOT) as the true value, and we rescale this sensitivity according to the sensitivity ratios we determined above.

Variation of the Spike

Since the central spike is allowed to vary in the different models, we can determine its variation from the data of Table 2.2. The ratio $f_{\rm j}/f_{\rm k}$ of the flux from the spike in a given band at two

Table 2.4: Calibrated Flux from the Spike.

Filter (1)	λ_{eff} (2)	f_{91} (3)	f_{93} (4)	f_{96} (5)
F175W	1970	···	15.4±1.2	8.4±0.7
F220W	2320	···	14.8±1.2	···
F275W	2800	···	17.7±1.3	8.2±0.4
F342W	3400	3.2±0.4	14.4±1.2	7.0±0.4
F502M	4990	7.0±0.8	···	···

Notes—Col. (1): FOC filter used in the observation; Col. (2): Effective wavelength of the filter in Å; Col. (3-5): Total flux from the spike in units of 10^{-18} erg s^{-1} cm^{-2} Å^{-1}.

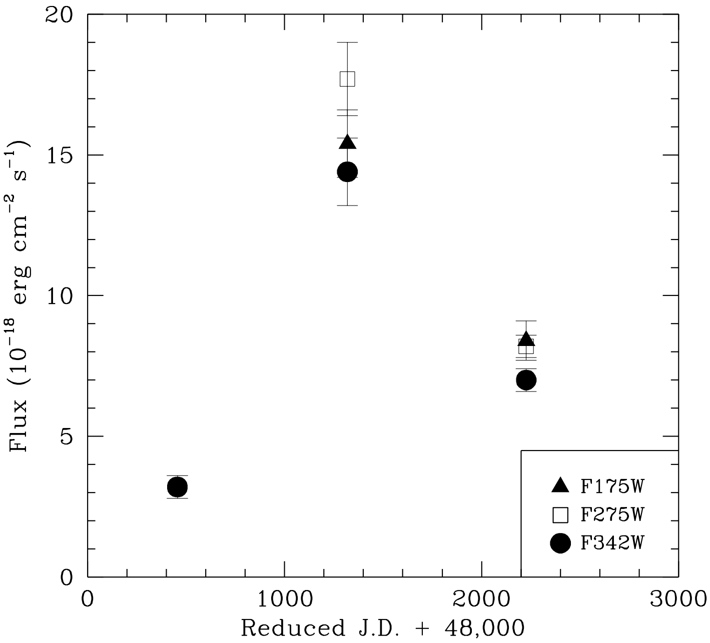

Figure 2.3: The light curve of the spike in the F175W, F275W and F342W passbands.

different dates can be computed from the equation below:

$$\frac{f_{\rm j}}{f_{\rm k}} = \frac{c_{\rm s}^{\rm j}\ I_{\rm b}^{\rm k}\ {\rm scale}_{\rm j}^2}{c_{\rm s}^{\rm k}\ I_{\rm b}^{\rm j}\ {\rm scale}_{\rm k}^2} \tag{2.4}$$

In Table 2.3 and in Figure 2.3 is presented the variation of the spike in all the bands where it has been possible to measure it. In table 2.4 the flux from the spike is shown in physical units. Note that, as will be discussed later, the spectrum of the spike is rather hot. For this reason the red-leak is negligible and we can convert from counts within one filter to erg s^{-1} cm^{-2} Å^{-1} at the effective wavelength λ_j of the filter by using the inverse sensitivity of that filter [$f(\lambda_{\rm j})$ = counts $U_{\rm j}/T_{\rm j}$].

As is evident, the center spike in NGC 4552 increased in luminosity by a factor of 4.5 from 1993 to 1996 confirming the results presented in Paper I. Moreover it appears that the spike

Table 2.5: FOS Observation Log.

Grating	λ range (Å)	Spectral Resolution (FWHM Å)	Date	Exp. (s)
G270H	2222–3277	1.89	24 May 1996	1240
G270H	2222–3277	1.89	24 May 1996	1110
G650L	3540–7075	23.4	24 May 1996	400
G780H	6270–8500	5.26	24 May 1996	430
G780H	6270–8500	5.26	24 May 1996	2410
G570H	4569–6818	4.02	16 Jan 1997	1380
G570H	4569–6818	4.02	16 Jan 1997	2410
G570H	4569–6818	4.02	16 Jan 1997	2410
G570H	4569–6818	4.02	17 Jan 1997	2410
G570H	4569–6818	4.02	17 Jan 1997	1690

faded from 1993 to 1996, decreasing in luminosity by about a factor of 2.0 at all observed wavelengths (1700–3500 Å).

2.3 FOS Spectroscopy

2.3.1 Observations

FOS spectra of the central spike of NGC 4552 were obtained on May 23, 1996 as part of the same HST/GO program (GO 6309), using the $0\farcs21\times0\farcs21$ square aperture (0.25–PAIR), the G270H, G650L and G780H gratings and the red FOS detector (FOS/RD). From the last FOS peak-up target acquisition stage we have verified that the spike was correctly centered to an accuracy of less than $0\farcs04$ in the FOS aperture. A subsequent FOS spectrum was obtained on January 16, 1997 on a different GO program (6099, PI: S.M. Faber) using the G570H grating and the same aperture and detector of our observations. We have retrieved this spectrum from the STScI archive to compare it with our data. A log of these observations is presented in Table 2.5.

All spectra have been calibrated by the standard STScI data pipeline. Note that the latest "Average Inverse Sensitivity" (AIS) method was used in the calibration. If more than one spectrum was available a weighted average has been used to compute the resulting average spectrum. For each output spectrum we also computed a companion "error spectrum," by properly combining the pipeline-supplied 1-σ error spectra. These error spectra are needed for the modeling of the spectral features described below.

2.3.2 The 1996 UV/Optical FOS spectrum

The 1996 UV-Dominated Continuum of the Spike

In Figure 2.4 we compare the 1996 merged FOS spectra of the central $0\farcs21\times0\farcs21$ region of NGC 4552 with a composite spectrum meant to represent the spectrum of the inner $r = 7''$ of this galaxy. The composite spectrum is obtained by combining the IUE spectrum of NGC 4552 (Burstein et al. 1988) with the low resolution (20 Å) optical spectrum of NGC 4649 (Oke et

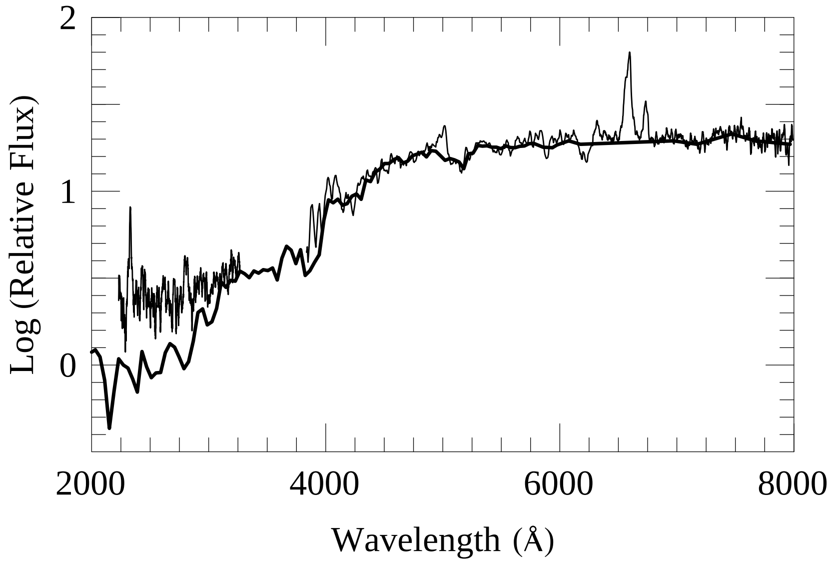

Figure 2.4: The overall 1996 FOS spectrum of NGC 4552 within the $0''.2 \times 0''.2$ aperture centered on the spike (thin line), is superimposed to a scaled combination of the IUE $10'' \times 20''$ aperture of NGC 4552 (Burstein et al. 1988) matched to ground-based optical spectrum of NGC 4649, a giant elliptical whose SED is virtually the same as that of NGC 4552 (Oke et al. 1981; thick line). The spectra have been normalized to the visual region. The FOS spectrum appears quite different owing to the appearance of UV and optical emission lines as well as a continuum UV excess shortward of $\lambda \sim 3000$ Å.

al. 1981), which is known to have a UV and optical SED very similar to that of NGC 4552 (cf. Burstein et al. 1988).

Normalizing at V magnitude, we see that this composite spectrum for the inner $7''$ of NGC 4552 is a very good match in overall spectral energy distribution for the FOS spectrum, with two notable exceptions: First, the FOS spectrum shows strong emission lines that are absent in the composite spectrum. Second, the UV SED of the FOS spectrum is far stronger than the IUE SED shortward of 3200 Å. The SED of the spike alone is obtained by subtracting the V-mag normalized $7''$ IUE spectrum from the $0''.21 \times 0''.21$ FOS spectrum (Figure 2.5). In the same figure we overplot the fluxes measured for the spike using the nominal filter sensitivities for the 1996 FOC observations, as well as blackbody SEDs for various temperatures. It is evident that both the FOC fluxes and the FOS SED agree well, and that together they indicate a temperature of $T \sim 15000$ K for the spike in 1996, if a thermal origin for the UV flux is assumed. In turn, this implies a bolometric luminosity of $\sim 3 \times 10^5$ $L_\odot$ for the spike (at a distance of 15.3 Mpc).

Defining The Emission Lines

The May 1996 FOS spectra of the central spike in NGC 4552, redshift-corrected, are presented in Figure 2.6. These data cover the range 2222–8500 Å, with a gap from 3277–3540 Å. The most prominent emission lines are identified. They include C II] λ2326, MgII λ2800, [O II] λ3727, [S II] λ4072, Hβ, [O III] $\lambda\lambda$4959, 5007, [N I] λ5700, [O I] λ6300, [N II] $\lambda\lambda$6548, 6583, Hα and [S II] $\lambda\lambda$6717, 6731.

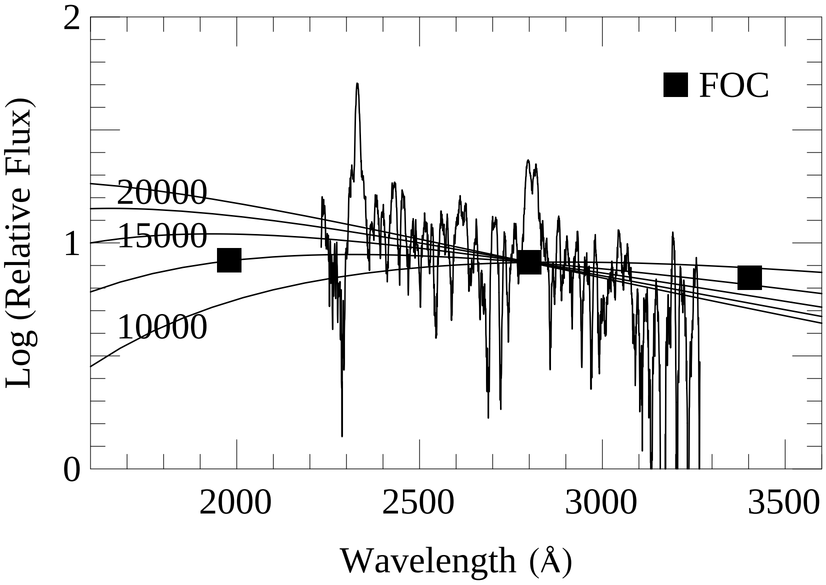

Figure 2.5: Comparison between the starlight-subtracted UV (G270H) portion of the 1996 FOS spectrum of the spike region and our FOC (F175W, F275W, F342W) UV photometry. The subtracted SED corresponds to the IUE spectrum shown in Fig. 2.4. The best match of both FOS spectrum and FOC photometry (filled squares) with the superimposed blackbody energy distributions is for $T \sim 15,000$ K. Moreover, such a comparison indicates that the UV continuum comes essentially from the unresolved spike.

Under the reasonable assumption that the emission line spectrum is from the spike alone, and the rest of the optical spectrum is underlying galaxy SED, by subtracting a suitable template for the galaxy SED we can get a good approximation to the spectrum of the spike. A suitable template spectrum can be found from the spectral library of Ho et al. (1995). After careful search for a "clean" galaxy spectrum (i.e., without apparent emission lines), we chose the spectrum of NGC 3115 on the basis both of high S/N and good overall SED match. (Obviously we would have preferred to use the Ho et al. spectrum of NGC 4649, but unfortunately it is of poor S/N.) The Ho et al. spectrum of NGC 3115 was then subtracted to the spectrum of NGC 4552 from the same library, and the result is shown in Figure 2.7. The very small difference between the two spectra testifies for the suitability of NGC 3115 as a template for the stellar SED of NGC 4552. The small positive difference in the spectral regions of Hα+[N II] and [S II] indicates that some emission is detected in NGC 4552 even within the large $2'' \times 4''$ aperture used by Ho et al.

Finally, the spectrum of NGC 3115 has been appropriately scaled both in flux and spectral resolution to the FOS spectra of NGC 4552, and subtracted to it. The resulting pure emission line spectrum is then taken as the spectrum of the spike on which we have conducted all subsequent analyses.

Diagnostics of the Spike Via Emission Line Ratios

Integration over all recognized emission lines with reasonable S/N has given the total flux in each of these lines, with the results being reported in Table 2.6. Figure 2.8 shows how the emission line ratios of the narrow components for the NGC 4552 spike compare to the

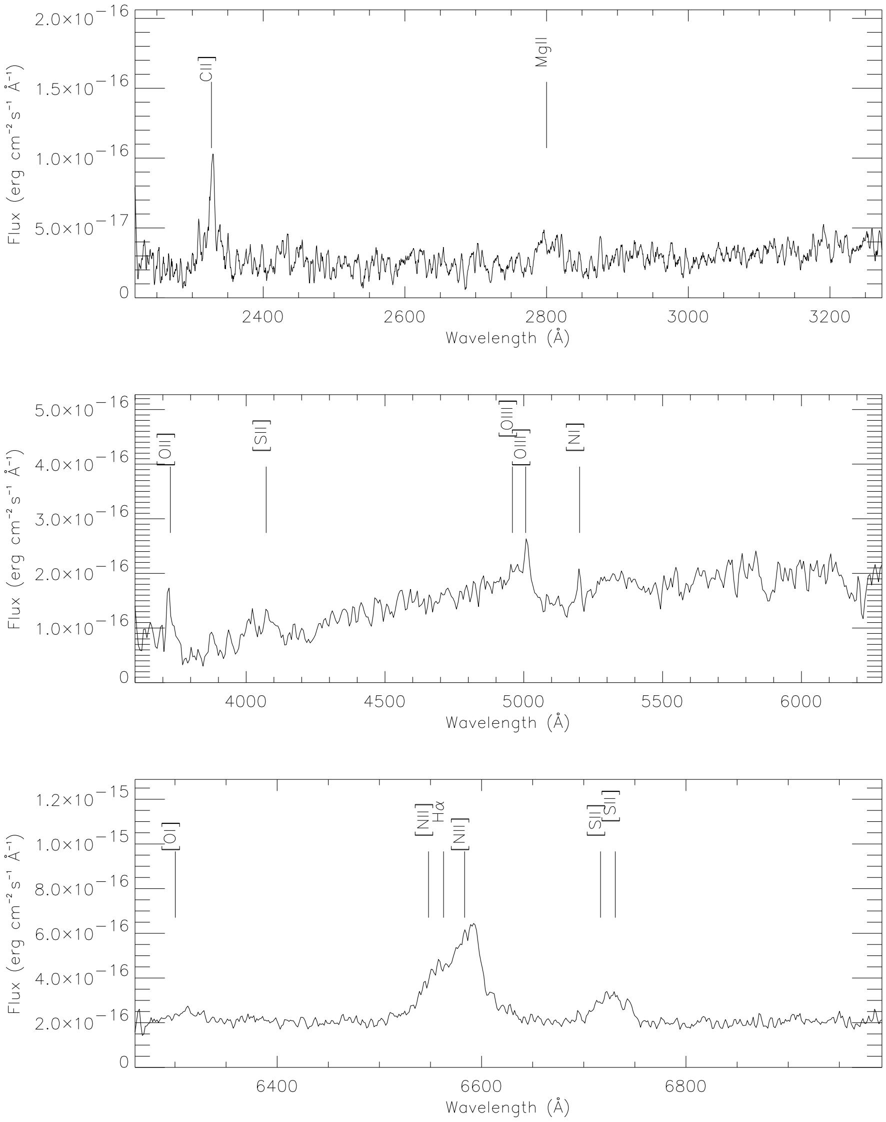

Figure 2.6: The 1996 HST/FOS spectra of the central $0\farcs2\times0\farcs2$ region of NGC 4552 . Each panel shows the spectrum from a different grating, in order of increasing wavelength (G270H, G650L and G780H). The spectra are slightly boxcar smoothed. Identification of the most prominent emission lines are given.

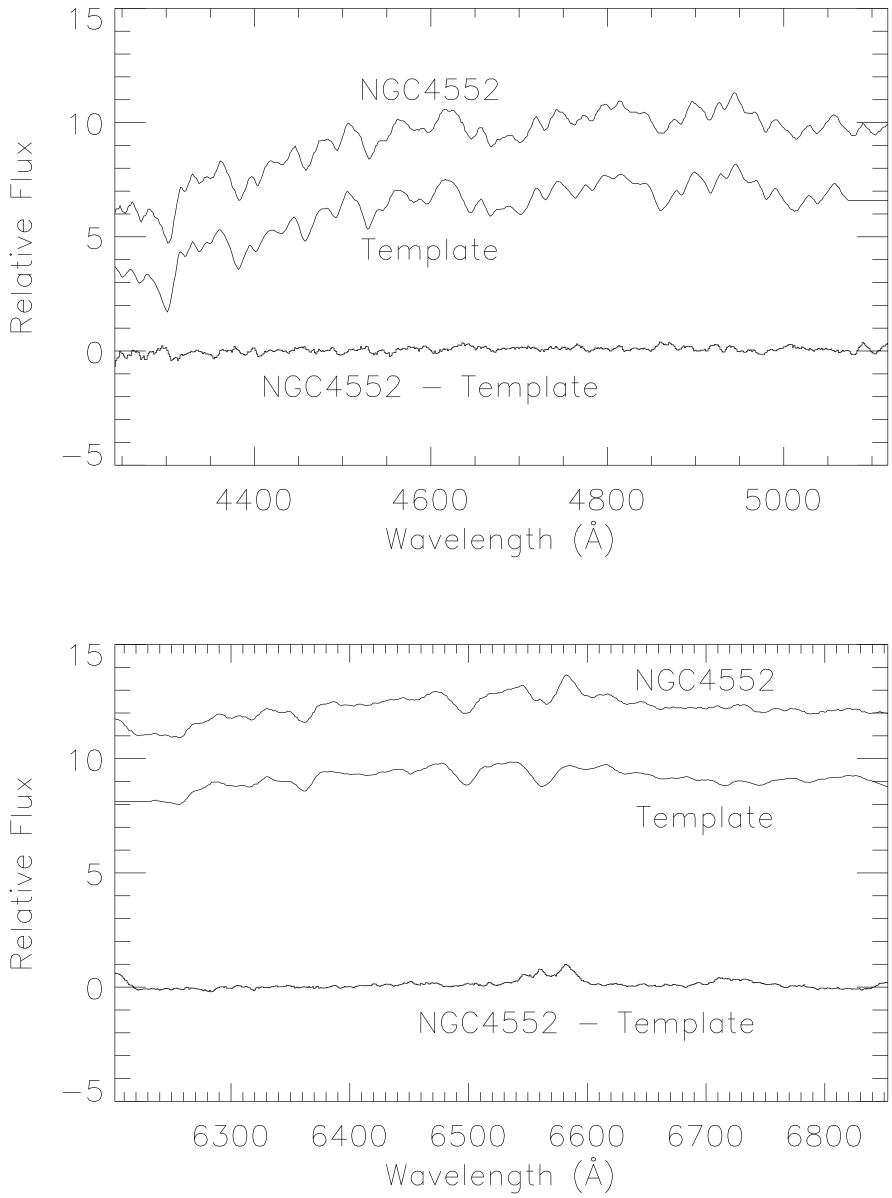

Figure 2.7: Underlying starlight subtraction from the spectrum of NGC 4552 by means of the adopted emission-free template spectrum (NGC 3115). Both spectra are from the library of Ho et al. (1995) and refer to an aperture of $2'' \times 4''$. Upper panel: the observed blue portion of the spectrum (top plot) is compared with the template (middle plot, offset by a constant), while the bottom plot shows the difference between the spectrum of NGC 4552 and the template. Lower panel: the same as in upper panel for the red portion of the spectrum. The excellent match in the spectral region free from emission lines fully justifies the choice of NGC 3115 as a template for starlight subtraction within the FOS aperture (note that a resolved Hα+[N II] emission emerges for NGC 4552).

Table 2.6: Line Emission Fluxes and Modeling Parameters

Spectrum (1)	Date (2)	Line (3)	Line Flux NLR (4)	BLR/NLR (5)	FWHM$_{NLR}$ (6)	FWHM$_{BLR}$ (7)	LOS v (8)
G270H	May 1996	C II] λ2326	3.5±1.1	2.8±1.3	680±230	4400±1000	600±75
G650L	"	Hβ	7.5±1.8	1.13±0.26[a]	963±75[a]	3060±260[a]	560±130
"	"	[O III] λ4959	9.2±2.0	"	"	"	"
"	"	[O III] λ5007	19.3±2.1	"	"	"	"
G780H	"	[O I] λ6300	11.7±1.7	1.13±0.26	963±75	3060±260	554±20
"	"	[O I] λ6363	4.5±1.0	"	"	"	"
"	"	[N II] λ6548	21.9±2.7	"	"	"	"
"	"	[N II] λ6584	65.7±8.1[b]	"	"	"	"
"	"	Hα	20.4±3.9	"	"	"	"
"	"	[S II] λ6716	18.1±2.8	"	"	"	"
"	"	[S II] λ6731	9.6±2.2	"	"	"	"
G570H	Jan. 1997	Hβ	5.08±0.35	2.07±0.18	731±40	4350±230	147±14
"	"	[O III] λ4959	4.40±0.39	"	"	"	"
"	"	[O III] λ5007	15.00±0.89	"	"	"	"
"	"	[O I] λ6300	7.63±0.67	1.90±0.22	714±35	2700±100	281±8[d]
"	"	[O I] λ6363	2.90±0.42	"	"	"	"
"	"	[N II] λ6548	17.9±1.3	"	"	"	"
"	"	[N II] λ6584	53.7±3.9[b]	"	"	"	"
"	"	Hα	12.7±1.6	"	"	"	48±44[c]
"	"	[S II] λ6716	11.9±1.2	"	"	"	281±8[d]
"	"	[S II] λ6731	8.6±1.0	"	"	"	"

[a] Since the S/N of this spectrum is low, these values have been held fixed at the values determined in the G780H spectrum.
[b] The ratio to the two [N II] lines has been forced to be exactly equal to the theoretical value 3.0.
[c] A proper fit to the Hα+[N II] complex could only be obtained by allowing the Hα components to have a different redshift from the other emission lines.
[d] These values have been constrained to be the same.

Notes—Col. (1): FOS grating used in the observations; Col. (2): Date the observation was taken; Col. (3): Identification of the emission line; Col. (4): Integrated flux in the Narrow Line Region (NLR) emission component in units of 10^{-16} erg s^{-1} cm^{-2}; Col. (5): Ratio between the flux in the Broad Line Region (BLR) and NLR emission components. The " in this column/line and others means that the parameters have been constrained to be the same as the last value specifically defined in this column; Col. (6): Measured Gaussian intrinsic velocity dispersion of the NLR line in units of km s^{-1}; Col. (7): Measured Gaussian intrinsic velocity dispersion of the BLR line in units of km s^{-1}; Col. (8): Observed redshift in km s^{-1}.

distribution of Seyfert galaxies, LINERS and H II regions in the diagnostic emission line diagrams of Ho et al. (1997). As is evident, the line ratios to Hα of [N II], [S II] and [O I] definitively place the spike in NGC 4552 among extreme AGNs, while the [O III]/Hβ ratio falls just on the borderline between Seyferts and LINERs. Therefore, the spike in NGC 4552 can be either classified as a very high excitation LINER or a very low excitation Seyfert.

2.3.3 Fitting the Emission Lines

The continuum-subtracted optical emission-line spectrum has been modeled as a whole by applying a specifically constructed IDL procedure which makes use of the Levenberg-Marquardt algorithm to fit a non-linear function. As usual in the case of AGN spectra, as a first-order approximation we have imposed on all the emission lines the following model constraints: [i] Each permitted *and* forbidden line consists of a narrow and a broad Gaussian component; [ii] the redshift of every emission line in a given FOS setup is assumed to be the same; [iii] the intensity ratio of the narrow and broad component is forced to be the same for all lines; [iv] the intrinsic width of all the broad and narrow components are constrained to be the same within a given spectrum. The one exception to these rules is the redshift of Hα in the 1997 G570H spectrum, which is found to be significantly different than that of the other emission

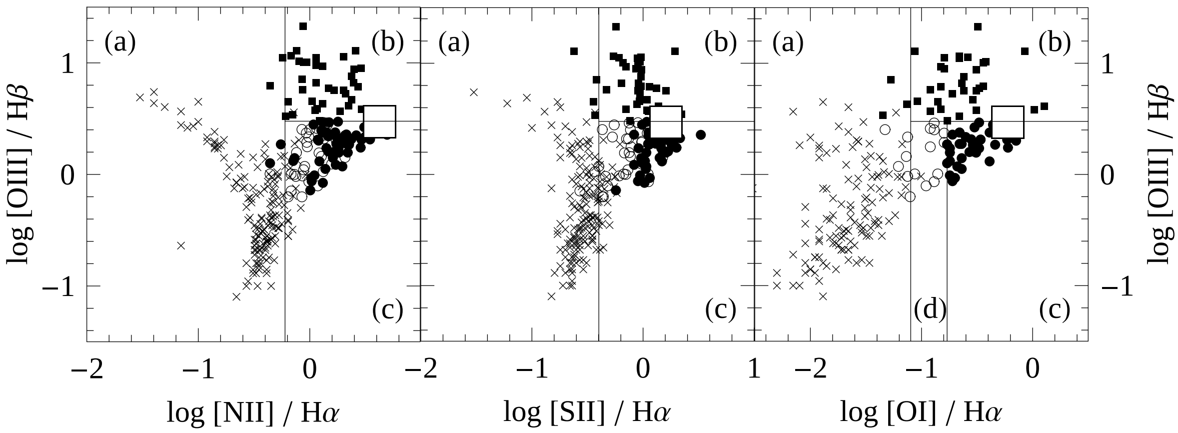

Figure 2.8: The location of the NGC 4552 nucleus (as derived from the narrow line emission components measured on the FOS spectra) on the diagnostic diagrams used by Ho et al. (1997); the large open square represents the position of NGC 4552 at the 1997 epoch. The corresponding errors are of the size of the smaller simbols. The 1996 data are consistent with the 1997 measurements, although with larger errors. The other symbols represent the nuclei included in the Ho et al. sample (crosses = H II nuclei, filled squares = Seyfert nuclei, filled circles = LINERs, open circles = transition objects). The vertical and horizontal lines delineates the boundary adopted by Ho et al. between (a) H II nuclei, (b) Seyfert galaxies, (c) LINERS and (d) Transition objects.

lines in this spectrum (see below). The derived parameters for the emission lines are given in Table 2.6. The 1-σ formal errors of the line parameters are estimated from the covariance matrix.

We first illustrate the case of the unresolved UV multiplet C II] λ2326 for which we assume a linear continuum under the emission line (i.e., no significant absorption under this feature). As demonstrated by Figure 2.9, the C II] emission clearly consists of both a narrow and a broad line component. Given the low S/N of the UV spectrum in this wavelength range, rather than taking a straight difference of observed minus model spectra, we show the reality of each component by applying a low pass filter (middle spectrum in Figure 2.9) and a high pass filter (lower spectrum). This result justifies our assumption [i] above.

The fits for the optical emission lines measured in the 1996 spectra are shown in detail in Figure 2.10. The region near Hβ and [O III] is shown from the G650L spectrum while the region from [O I] to [S II] is shown from part of the G780H spectrum. The top plot referring to each region/grating combination shows the spectrum as observed, together with the spectrum of the template; the middle plot shows the emission lines fitted to the template-subtracted spectrum; and the bottom plot shows the residuals (observed spectrum minus model fit). The same is shown in Figure 2.11 for the emission lines in the 1997 G570H spectrum.

The models fit the data quite well, as can be seen both by eye and from the values of the reduced chi-square χ^2_ν given for each fit. In each case and for both 1996 and 1997 data we see that the emission lines require both a narrow and broad line component.

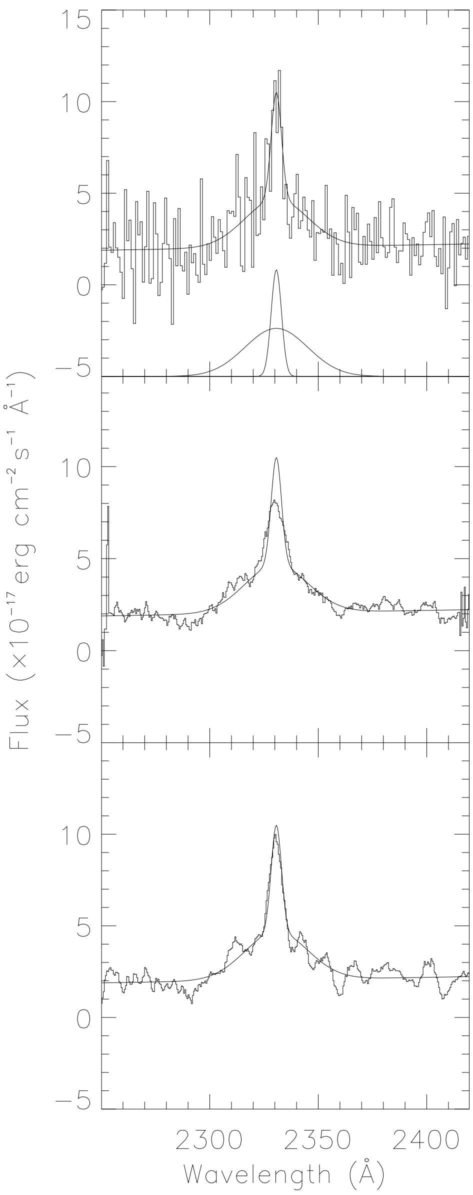

Figure 2.9: Upper panel: The portion of original UV (G270H) spectrum containing the C II] λ2326 Å multiplet with superimposed our best-fit model; individual components of the model are shown at the bottom of the panel. Middle panel: the best-fit model is overplotted on a 19 pixel, boxcar-smoothed version of the spectrum; Bottom panel: the same best-fit model is superimposed to a 37 pixel, 4th degree Sawizki-Golay filtered spectrum. The adopted filterings applied to the original spectrum as shown in the two lower panels are meant to emphasize the broad and narrow component, respectively. The reduced chi-square for the fit in the upper panel is $\chi^2_\nu \simeq 1.06$.

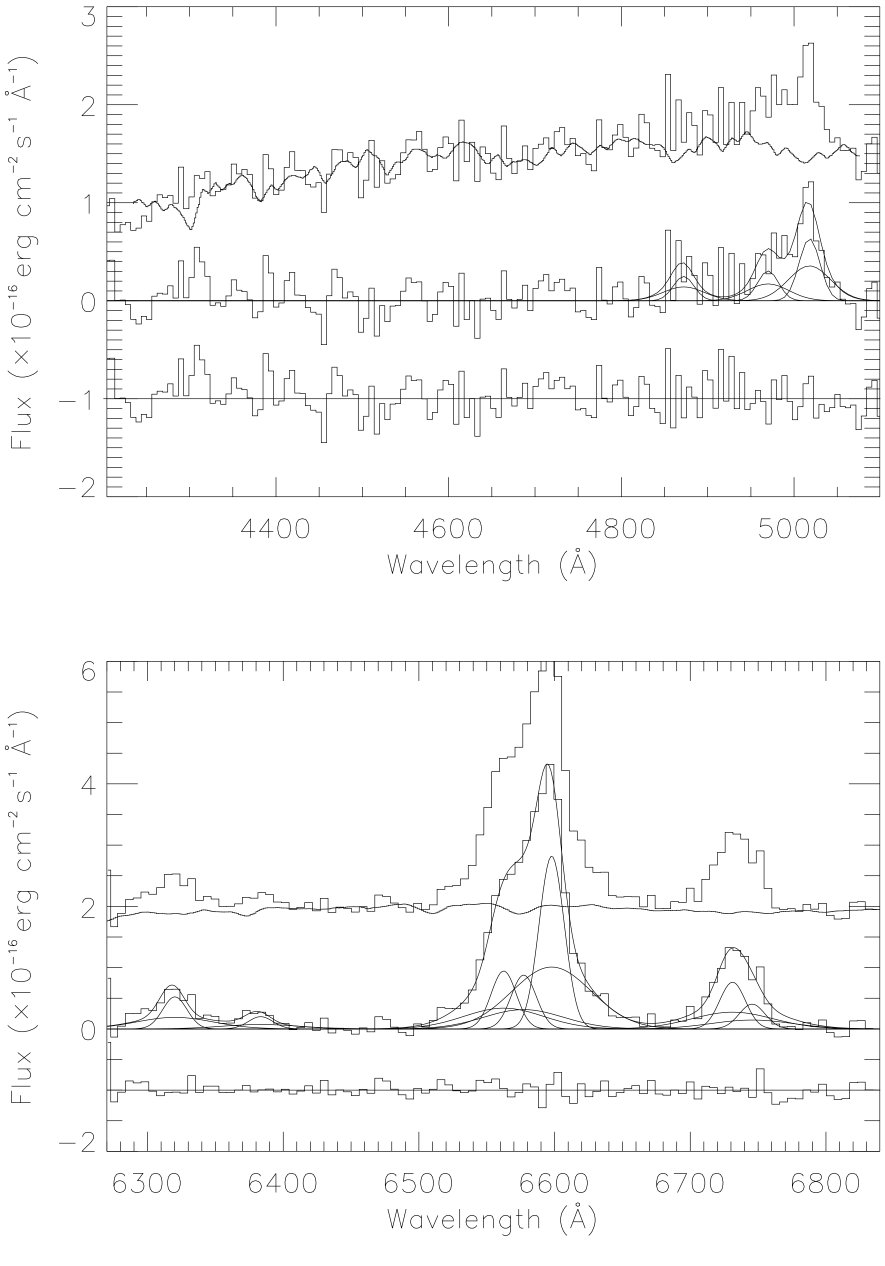

Figure 2.10: Upper panel: gaussian decomposition of the Hβ and [O III] lines from the FOS G650L spectrum of the center of NGC 4552. In the top plot the adopted emission-free template is superimposed to the original spectrum. The middle plot represents the starlight-subtracted spectrum with superimposed our best-fit Gaussuan model as well as the individual (narrow and broad) components. The residuals (arbitrarily shifted) are shown at the bottom of the panel. Lower panel: the same as in upper panel for the [O I], [N II], Hα, and [S II] lines in the red region of the FOS G780H spectrum, rebinned over 4 pixels. Owing to the low S/N of the G650L spectrum the lines included in in this range have been modeled imposing the same gaussian parameters obtained from the lines in the G780H spectrum, hence determining only redshift and line fluxes. The reduced chi-square for the fit in the upper panel is $\chi^2_\nu \simeq 1.23$, while for the lower panel fit $\chi^2_\nu \simeq 1.00$.

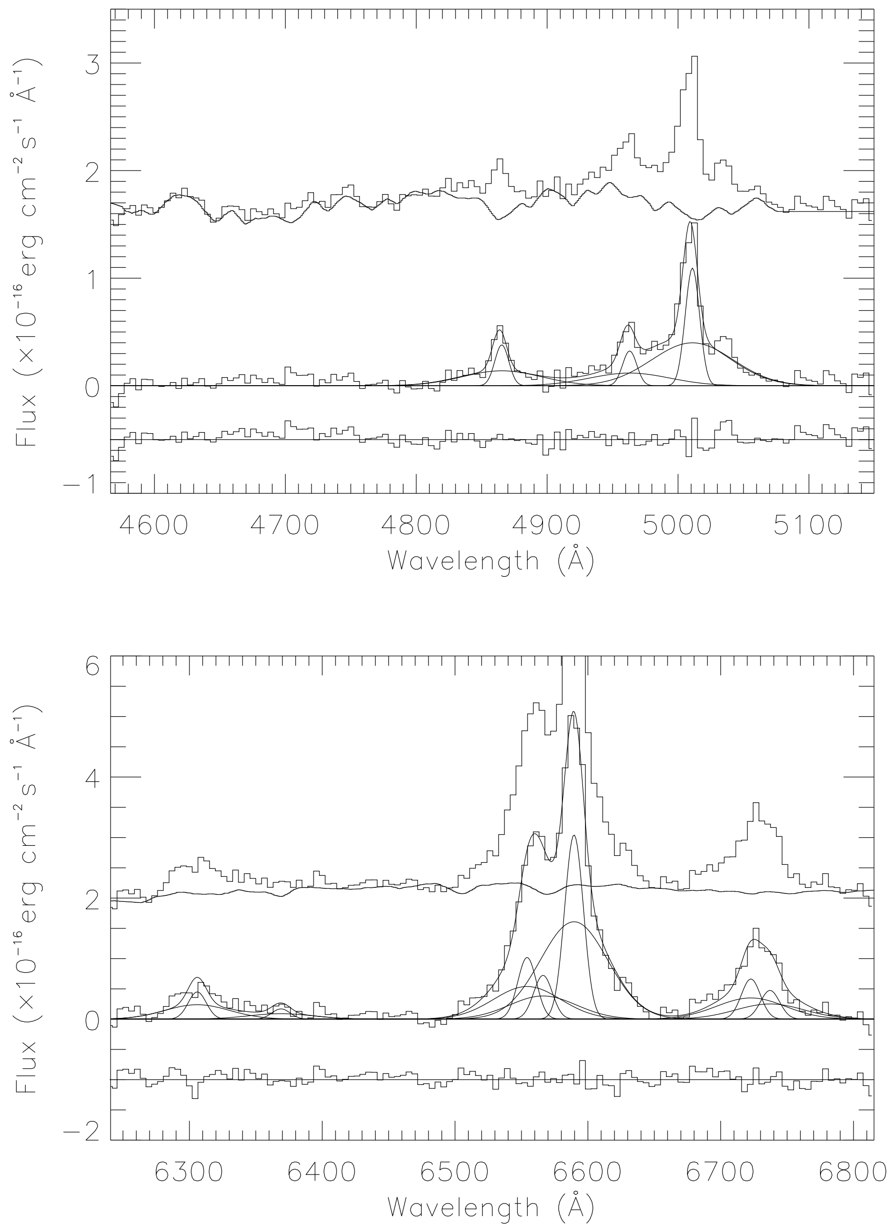

Figure 2.11: The same as in Fig. 2.10 for the FOS G570H spectrum (here rebinned over 4 pixels) obtained by Faber and collaborators in January 1997. In order to get a satisfactory fit of the Hα+[N II] complex, a blueshift by 4.6 Å ($\sim$ 230 km s^{-1}) of both components of Hα was required with respect to both 1996 and to the 1997 position of the [N II] doublet. For the fit in the upper panel $\chi^2_\nu \simeq 1.35$, while in the lower panel $\chi^2_\nu \simeq 1.37$.

2.3.4 Results from the Emission Line Measures

An examination of the results of the emission line fits given in Table 2.6 permits us to draw the following significant conclusions: [i] Satisfactory fits of the emission lines identified in nuclear FOS spectra taken ~ 8 months apart can be obtained only by resorting to a combination of broad and narrow components for both the permitted as well as the forbidden lines. This result is at variance with the behavior of classical AGNs – where the broad component is usually present only in the permitted lines. [ii] The emission lines are very broad, with fits indicating very high velocity widths for both the broad (FWHM $\simeq 3000$ km s^{-1}) and narrow components (FWHM $\simeq 700$ km s^{-1}). [iii] The shape of the Hα+[N II] complex has definitely changed from the May 1996 spectrum to the January 1997 spectrum. There is indeed an obvious "dip" in the middle of the Hα+[N II] complex that is clearly not present in the 1996 spectrum. Within our procedure, a satisfactory fit can be formally achieved only allowing for a shift to the blue of ~ 230 km s^{-1} of the whole (narrow + broad) Hα line in the latter spectrum compared to the former one. This also implies a similar shift of the Hα components with respect to the [N II] lines in the 1997 spectrum, while no hint of such a difference in radial velocity is seen in the 1996 spectrum.

2.4 Discussion

The phenomenology we have described in detail in the previous sections can be summarized as follows: [i] The central spike UV luminosity has varied by a factor of a few over timescales of order of 15 months, being in the range from 10^5 to 10^6 L$_\odot$. [ii] An offcenter UV spike is present only in the 1991 data. [iii] The spectrum of the spike is characterized by a strong UV continuum plus moderate excitation emission lines. [iv] The emission line ratios are typical of AGNs, but unusual in that both permitted and forbidden lines require broad and narrow components. [v] The baricenter of the Hα emission has changed by ~ 230 km s^{-1} between May 1996 and January 1997.

This complex phenomenology clearly points towards the presence of a very weak AGN at the center of this galaxy, most likely powered by a low level of accretion onto a central black hole (BH). Other interpretations (a central supernova, a central starburst, ...) were already considered unlikely, given the early evidence (Paper I, Renzini 1995). The additional HST evidence gathered in 1996 is reasonably conclusive in this respect.

2.4.1 Is the Nucleus of NGC 4552 the Least Luminous Known AGN?

With the adopted distance to the Virgo cluster of 15.3 Mpc and the observed flux of the broad Hα emission from Table 6, the broad Hα luminosity is $\sim 5.6 \times 10^{37}$ erg s^{-1}. This is a factor of two less than the broad Hα luminosity of the nearest known AGN, the Seyfert 1 nucleus of NGC 4395, and a factor of ~ 20 less luminous than M81, the next faintest Seyfert 1 nucleus (Filippenko, Ho, & Sargent 1993). Filippenko et al. adopt a distance to NGC 4395 of 2.6 Mpc, and clearly claims of which of the two nuclei is the least luminous have to cope with the uncertainty in the relative distance of the two galaxies. It is beyond the scope of this Chapter to explore this aspect in detail, but it is safe to conclude that given the current evidence NGC 4552 is likely to harbor the intrinsically faintest known AGN, or at least the next to the faintest AGN. Of course, allowance should also be made for the confirmed variability of the mini-AGN in NGC 4552.

A comparison of the ultraviolet FOS spectra of the NGC 4552 spike and the FOS spectrum of the AGN in NGC 4395 (Filippenko, Ho & Sargent 1993) shows that the latter contains lines of high ionization that are not present in the former. In particular, Filippenko et al. point out that the existence of the Bowen fluorescence mechanism from OIII 3133 to HeII 3204 is a good diagnostic of the existence of high ionization in an AGN. These two lines are notably absent in the FOS G270H spectrum of the spike in NGC 4552, as are other high level Fe and Ne lines commonly seen in high ionization AGN. However, the C II] and MgII lines have similar intensities in the two objects, while the flux of the UV continuum is decreasing towards shorter wavelengths in NGC 4395 in the spectrum of Filippenko et al., but it is increasing in our spectrum of the spike in NGC 4552.

Ground based spectroscopic observations of NGC 4395 in the Hα+[N II] region have been obtained by Filippenko & Sargent (1989, FS89) using a $2''$ aperture. Given the relative distances of the two galaxies, our FOS and FS89 observations sample regions of quite similar physical size. According to FS89, the narrow line and broad line components of Hα+[N II] in the nucleus of NGC 4395 have FWHM of ~ 60 and ~ 800 km s^{-1}, both much narrower than in the case of the mini-AGN in NGC 4552. We conclude that the arguments developed by Filippenko et al. to exclude explanations other than BH accretions for the activity in NGC 4395 are even more effective in the case of NGC 4552, which shows more extreme AGN characteristics.

2.4.2 Why is the AGN Luminosity so Low?

As already suggested in Paper I, the phenomenology of the spike in NGC 4552 is generically consistent with the scenario in which a central, UV-bright flare is caused by the tidal stripping of a star in a close flyby with a central supermassive BH. From the theoretical point of view, only the extreme case of a total disruption of a $\sim 1\,M_\odot$ main sequence star has been widely investigated so far (e.g., Rees 1988, 1990; Evans & Kochanek 1989; Luminet & Barbuy 1990; Cannizzo, Lee, & Goodman 1990; Kochanek 1994; Eracleous et al. 1995; Loeb & Ulmer 1997; Ulmer 1997a,b).

The frequency of such events is estimated to be of one total disruption every $\sim 10^3 - 10^4$ yr in typical giant elliptical galaxies (Rees 1988, 1990). The flare is predicted to be very bright for several years ($\sim 10^{10} L_\odot$), much brighter than the observed flare. This indicates that if the flare in NGC 4552 was caused by a tidal stripping in a BH-star flyby, then this flyby was rather wide, and led to only partial stripping. Obviously one expects wider flybys to be vastly more frequent than the hard ones causing total disruption. To be consistent with the observed luminosity, only $\sim 10^{-3} M_\odot$ should have been stripped, as the flare luminosity is predicted to scale with the 5/3 power of the mass of the accretion disk (Cannizzo et al. 1990; Paper I).

Tidal stripping of a star is but one possible way to feed matter to a massive central BH at a low rate. Other mechanisms include: a) Roche lobe overflow from one or more stars in bound orbit(s) around the BH (Hameury et al. 1994); b) accretion from a clumpy interstellar medium near the central BH; or c) gas fed to the BH via a cooling flow within the X-ray emitting hot interstellar medium known to exist in NGC 4552.

Some circumstantial support for accretion from a clumpy ISM may come from NGC 4552 showing extended Hα emission in the inner 2 kpc (Trinchieri & di Serego Alighieri 1991), possibly due to the recent accretion of a dwarf galaxy. Concerning alternative c) above, we note that the large dispersion in the X-ray luminosity of elliptical galaxies for a given optical luminosity argues for the hot gas flow in most ellipticals being directed outwards, i.e. being in either a supersonic wind or subsonic outflow regime (Ciotti et al. 1991; Renzini 1996). However, even when gas flows out through most of the galaxy body, a mini-inflow is likely to be established in the innermost ($r \lesssim 300$ pc) regions, with inflow rates being as low as a few $10^{-3} M_\odot$ yr^{-1} (Ciotti et al. 1991). Accretion onto the central BH is likely to be intermittent (Ciotti & Ostriker 1997), hence resulting in sizable excursions in the associated luminosity (flickering), a well known phenomenon among AGNs (Ulrich, Maraschi, & Urry 1997).

It may well be that each of all of these feeding mechanisms operates from time to time in the central regions of elliptical galaxies like NGC 4552. Theoretical models of the various options all must end up with assuming that an accretion disk is established, and from this point on all options resemble each other very closely. From the observational point of view, the available data do not allow a clear cut discrimination among which of these alternatives is responsible for the event in NGC 4552.

However, circumstantial evidence in favor of the tidal stripping option comes from the noticed shift in the broad Hα emission between May 1996 and January 1997. Tidal stripping/disruption is indeed predicted to give rise to an *elliptical* accretion disk, the precession of which results in sizable Hα line profile variations (Eracleous et al. 1995). This scenario (tidal stripping plus elliptical disk) has been proposed to account for the observed variability of the broad Hα line profile in the active nucleus of NGC 1097 (Eracleous et al. 1995; Storchi-Bergmann et al. 1995, 1997).

2.4.3 Origin of the Broad Forbidden Lines

According to general wisdom, the onset of broad forbidden-line emission in AGNs is prevented by the high densities existing in broad line regions (BLR). The BLR is thought to be close to the central BH, and most likely consisting of an accretion disk around it. The narrow-line region (NLR) is thought to be located further away from the central BH, and likely consisting of lower density clouds being illuminated by the radiation cone emerging from the disk.

We preliminarily note that a low density in the accretion disk is demanded by the very low luminosity of the mini-AGN in NGC 4552. As such, nothing may prevent the forbidden lines to originate from the disk itself, rather than from a physically distinct region. If so, our modelling of the emission lines as a unique combination of a broad and a narrow component may be adequate as a first approximation, but may fail to represent the actual geometry of the emitting region. If the whole emission line radiation originates from a (thin) disk, then the gradient in rotational velocity should be responsible for the actual line profile, with the broadest part of it originating in the inner regions of the disk, with a continuous transition to a narrower and narrower emission towards its outer regions. However, given the low S/N of the FOS spectra we do not consider worth venturing here into more sophisticated line profile modelling based on detailed accretion disk models.

2.4.4 Setting Constraints on the Mass of the Central Black Hole

The size of the emitting region that is responsible for the spike can be estimated in two ways. As noticed in Section 2.2.3, the profile of the central spike in the 1996 images is consistent with that of the PSF of the FOC. An upper limit to the size of the emitting region has been obtained by convolving the PSF with a series of Gaussian profiles of various widths. With Gaussian FWHM of $0\farcs03$ one notices that with the S/N corresponding to our data the profile starts to depart appreciably from the PSF. We therefore adopt an upper limit of 0."03 for the size of the emitting region, which corresponds to $R = 1.1$ pc. Assuming a rotation velocity of 1100 Km s^{-1} (this is the σ_v =FWHM/$\sqrt{8\ln 2}$ measured on the G570H spectrum), a rough upper limit to the mass of a central compact object then follows: $M \lesssim Rv^2/G \simeq 2 \times 10^9$ M$_\odot$.

Alternatively, the size of the broad line emitting region can be estimated from the upper limit to the density as set by the forbidden lines, and by the Hα luminosity. Following Osterbrock (1989)

$$V = \frac{L(\mathrm{H}\alpha)}{f\ n_\mathrm{e}^2\ \alpha_{\mathrm{H}\alpha}^{\mathrm{eff}}\ h\ \nu_{\mathrm{H}\alpha}},$$

where V is the volume occupied by the emitting gas, $L(H\alpha)$ is the total luminosity of the broad $H\alpha$ line, f is the volume filling factor, n_e^2 is the gas electron density, $\alpha_{\mathrm{H}\alpha}^{\mathrm{eff}} = 1.17 \times 10^{-13}$ cm^3 s^{-1}, h is the Planck constant and $\nu_{\mathrm{H}\alpha}$ the frequency of the $H\alpha$ line.

From the presence of the broad [S II] forbidden lines we know that $n_\mathrm{e} \lesssim 10^4$ cm^{-3}. By assuming that the gas is uniformly distributed within a sphere and a unity filling factor we get a lower limit to the radius of the emitting region, i.e., $R \sim 0.2$ pc. More likely the emission comes from bound material orbiting around a central mass, hence $M \gtrsim Rv^2/G \simeq 3 \times 10^8$ M$_\odot$.

Finally another constraint to the size of the emitting region comes from the variability of the spike. From the time scale $t \simeq 2$ yr one can say that the emitting region should be smaller than $R \lesssim 0.6$ pc, which is of the same order of magnitude and consistent with our previously determined values.

Our rough estimate, between 3×10^8 to 2×10^9 M$_\odot$ is consistent with the mass of $M \simeq 4 - 6 \times 10^8$ M$_\odot$ of the supermassive central BH in NGC 4552, obtained by Magorrian et al. (1998), using simple *isotropic* dynamical models based on HST photometry and ground based kinematics.

2.4.5 A Possible Explanation For the Disappeared Offcenter Spike

In 1991 the offcenter spike was as strong as the central one which later flared-up in 1993. It might have been a mere 4σ statistical fluctuation, or a nova, a stellar collision, or whatever; we may never know. But what if a relation exists between the offcenter spike and the now–confirmed presence of a mini-AGN just ~ 10 pc away?

As stated in the Introduction, we know that the surroundings of the center of NGC 4552 exhibit a quite complex phenomenology, with extended Hα emitting gas (Trinchieri & di Serego Alighieri 1991) and a dust ring (Carollo et al. 1997a,b). Relativistic jets are well-known phenomena associated with AGN, emerging perpendicular to the accretion disk (e.g. Blandford et al. 1991). It is therefore reasonable to hypothesize that a jet can be produced each time an accretion event feeds the supermassive central BH. Such a jet by impacting against a relatively dense and cold cloud, could shock heat the cloud material, producing an optically bright transient source.

Figure 2.12 shows the $V-I$ (F555W-F814W) color map of the central regions of NGC 4552. The two optical WFPC2 images were obtained on January 1997 (PI S. Faber). The images are preliminarily reduced by the standard STScI data pipeline, then coadded using the IRAF/STSDAS task CRREJ. The resulting color map is resampled onto a finer grid by means of bilinear interpolation to smooth the pixellated appearance of the image. The photometric zero point is converted to the Johnson-Cousins system following the procedures described by Holtzman et al. (1995).

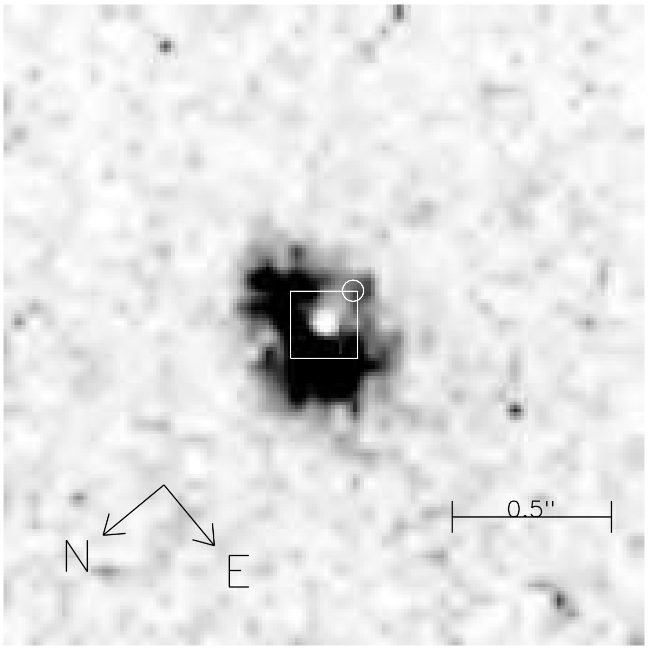

Figure 2.12: The $V-I$ (F555W-F814W) color map of the central regions of NGC 4552. The two optical WFPC2 images were obtained on Jan. 1997. The darkest color correspond to $V-I \simeq 1.44$ mag, while the background is at the $V-I \simeq 1.34$ mag level. The central square represents the size of the $0\farcs2 \times 0\farcs2$ FOS aperture used for the spectroscopic observations. The central spike is clearly visible as a bright spot, and the position of the offcenter spike present only in the 1991 data is indicated by the open circle.

An inhomogeneous ring-like feature clearly emerges with its inner edge at $\sim 0\farcs1 - 0\farcs2$ from the center. This ring is redder than the surrounding galaxy background with $(V-I) \simeq 1.34$, reaching a peak color difference at P.A.=45° of $\Delta(V-I) \simeq 0.10$, or $E(B-V) \simeq 0.09$. The likely interpretation of this feature is that we are seeing an obscuring dusty ring circling the central spike that is unobscured as indicated by the Balmer decrement in the FOS spectra which is consistent with no absorption.

It is interesting to note that the position of the 1991 offcenter spike ($\sim 0\farcs14$ from the center) places it *just* on the inner edge of the ring, and it is tempting to speculate that the offcenter spike in the 1991 image could be the result of a transient nuclear jet impinging on this dusty ring.

Incidentally, it is also interesting to note that the central spike is clearly seen as a point-like source in Figure 2.12. The F555W and F814W band flux reported by Carollo et al. (1997a) for this spike is consistent with being due uniquely to the line emission (mostly Hα+[N II]) as measured on our FOS spectra, when convolving it with the transmission curve of the filters and the QE of the detectors.

2.4.6 Central Spikes in Other Galaxies

Pre-COSTAR, deconvolved HST observations of an unbiased sample of early type galaxies has shown that up to $\sim 25\%$ of them may exhibit a central spike in the visible, in excess of the nuker law (Lauer et al. 1995). Maoz et al. (1996) show that, in FOC images that random sample the cores of 110 nearby galaxies in the ultraviolet, $\sim$ 10% show a unresolved point source in their centers. In the Carollo et al. (1997a,b) sample of 18 ellipticals (mostly with kinematically distinct cores) 4 exhibit a central spike in optical WFPC2 images, one of which is NGC 4552.

The question that naturally arises is whether any of these other central spikes are flares caught at some phase in their development. This is a non-trivial question, as we know of at least one other galaxy, the Sa galaxy NGC 2681, which has a UV-bright, unresolved core that is *not* a flare (Cappellari et al. 1998). We see at least two possible origins for central spikes that are not due to accretion onto a massive BH: a recent burst of star formation or stellar coalescence in a very high density environment. Both options are currently being entertained for the origin of the central cluster of hot stars in the nucleus of our own Galaxy (Genzel et al. 1994), with many such stars exhibiting Wolf-Rayet type spectra. This central cluster shares two relevant properties with some of the spikes mentioned above: a sub-parsec size, and a luminosity $\sim 10^7\,\mathrm{L}_\odot$, well in the range covered by them. Seen from the distance of the Virgo cluster, the bulge of our own Galaxy would also show an unresolved, UV-bright central spike!

As mentioned in the introduction, a point like source (at the HST pre-COSTAR resolution) was also detected at the center of the bulge of the Sa galaxy NGC 2681 (Bertola et al. 1995). FOC and FOS observations similar to those of 1996 reported here for NGC 4552 were also obtained for this galaxy, and reveal that no excess exists over a pure nuker law of the power law type (Cappellari et al. 1998).

2.4.7 Yet Another Way to Search for Central Black Holes in Galaxies

In Section 2.4.2 we have discussed various possibilities for feeding a central supermassive BH in galactic spheroids. Such masses sit at the bottom of the gravitational potential well of a galaxy, where stellar and ISM densities reach their maximum, and where any cannibalized material tends to converge. As such, one is tempted to say that the real problem is how to *avoid* a low, fluctuating level of accretion onto a massive BH — hence of low level AGN activity — rather than how to produce it. We actually argue that wherever a massive BH exists, it is likely to be accompanied by at least a weak level of *activity*.

The case of NGC 4552 offers a lesson in this respect. Thanks to its angular resolution, HST observations in either UV or optical imaging or narrow aperture spectroscopy allow to reveal mini-AGN activity which would be essentially invisible with similar ground based observations. Therefore, besides the stellar and gas dynamical techniques mentioned in the introduction, HST observations similar to those conducted on NGC 4552 can help to reveal the presence of central BHs in galactic spheroids.

It is the angular resolution properties of HST that make it so valuable in the search for nuclear spikes. A similar high resolution capability is now within reach also from the ground at near-IR wavelength, as a result of adaptive optics (AO) developments. AO-fed, near-IR, narrow aperture spectroscopy of the center of galactic spheroids might reveal broad emission lines of the Paschen and Brackett series, hence potentially offering additional opportunities for the demography of central BHs in galactic spheroids.

This is indeed a subject of great interest in the context of galaxy formation and evolution. Only few galaxies may indeed host a massive BH in hierarchical models in which most of star formation takes place in small galaxies, and it is the late merging of these entities that leads to the formation of massive spheroids. However, central massive BH may be more ubiquitous in other hierarchical models in which most of the merging activity takes place at early times, among mostly gaseous components, and such merging is accompanied by intense star formation and dissipational collapse in the central regions. As noted in the Introduction, central massive BHs seem to be present in most spheroids, which together with the noted tight relation between the mass of the BH and the mass of the spheroid seem to argue in favor of the latter scenario of spheroid formation.

2.5 Conclusions

By virtue of the normal elliptical galaxy NGC 4552 having been multiply observed with HST via imaging (in 1991, 1993 and 1996) and via spectroscopy of its nucleus (1996, 1997), we appear to have caught in mid-action a transient accretion event onto the central supermassive black hole of this galaxy.

This accretion reveals itself in several ways:

1. A central, unresolved (at the $0\farcs03$ level) ultraviolet-bright source was first detected in 1991, it increased in luminosity by a factor of ~ 4.5 by 1993, and then declined a factor of ~ 2.0 by 1996. Based on its UV spectral energy distribution, we estimate its 1996 luminosity to be $\sim 3 \times 10^5 L_\odot$ and its temperature to be about 15,000 K.

2. The FOS spectrum of this source taken in May 1996 shows a Seyfert/LINER type of emission line spectrum, with both permitted *and* forbidden lines being best modelled by the combination of broad (FWHM $\simeq 3000$ km s^{-1}) and narrow (FWHM $\simeq 700$ km s^{-1}) components. Nevertheless, the low luminosity of the broad Hα component ($\sim 5.6 \times 10^{37}$ erg s^{-1}) makes the central spike in NGC 4552 likely to be the least luminous among all know AGNs.

3. The FOS spectrum taken in January 1997 shows quite similar characteristics, except that the radial velocity of the Hα emission has shifted blueward by ~ 230 km s^{-1} compared to the spectrum taken in May 1996.

4. The 1991 UV image shows a second spike, offset by $0\farcs14$ from the central one, which does not appear in later images. We speculate that this second spike could be due to dense gas in the dusty ring seen at nearly the same distance having been shocked by a relativistic jet emerging from the central mini-AGN, possibly produced by a previous accretion event.

From these observations we can constrain the mass of the supermassive black hole in the center of NGC 4552 to be between 3×10^8 to 2×10^9 $M_\odot$, consistent with ground-based estimates. We discuss various possibilities for the source of matter that can produce an AGN that is as low in luminosity as this mini-AGN in NGC 4552. Partial tidal-stripping of a star in a close fly by with the black hole is an obvious possibility, but other interpretations cannot be excluded. These include accretion of clumpy gas that is seen near the center of the galaxy, or from a mini-inflow gas fed by the X-ray emitting hot gas in the galaxy. However, the change in the radial velocity of Hα over a 8 month period is most consistent with a partial tidal stripping event.

It is likely that most spheroids harbor a central massive black hole, as suggested by recent observations (cf. Kormendy & Richstone 1995; Magorrian et al. 1998; Ho 1998). If so, given all the above mentioned opportunities for a low, fluctuating rate of mass accretion onto such black holes it appears that transient mini-AGN activity similar to that we have discovered in NGC 4552 should be a widespread phenomenon. Indeed, it is quite conceivable that each of all mentioned mechanisms – tydal stripping, accretion from a clumpy ISM, accretion from a mini-inflow – are occasionally at work in real galaxies. While order of magnitude estimates of the duration and frequency of such events might be guessed from a theoretical viewpoint, we believe that first expanding the empirical evidence will be more rewarding in the near future.

HST high resolution UV imaging and narrow aperture spectroscopy with either HST of with adaptive optics from the ground should allow to detect in other galaxies signs of similar mini-AGN activity. This will offer yet another opportunity to expand the demography of central massive black holes in galactic spheroids, as well as to study virtually unobscured black hole accretion phenomena at a different regime compared to more powerful AGNs.

Acknowledgements

MC is grateful to the European Southern Observatory for its kind ospitality in the period during which much of the HST data analysis has been completed.

2.6 Appendix

2.6.1 Nonlinearity Correction of a Non-Uniform Background

Flat field nonlinearity of the FOC has been known for a long time and has been well-characterized (Jedrzejevski 1992). The true count rate ρ can be derived from the observed count-rate r by inversion of the following equation, which describes the behavior of the linearity relation for intensity values up to $\sim 80\%$ of the saturation value a

$$r = a\ (1 - e^{-\rho/a}) \tag{2.5}$$

where a is a fitting parameter that has been determined from actual measurements. $a = 0.73$ for the 512×512 F/96 observing mode and $a = 0.11$ for the 512z×1024 mode (de-zoomed pixel!) (Nota et al. 1996).

It has also long been known that point sources remain in the FOC linear range up to values $\sim 8\times$ higher than those for the flat field. This has lead for example in the FOC Handbook (Nota et al. 1996) to the simple guideline for observer to "keep the count rate in the central pixel below 1 count/sec," to get reliable photometry of point sources in the 512×512 mode.

It was not so clear what to do in the intermediate cases of a non-uniform background, as is always the case with the galaxies surface brightness photometry. In some cases the above guideline was still adopted, leading to severe underestimation of the nonlinearity effect (eg. Crane et al. 1993), as will be shown below.

Greenfield (1994) presented a simple method to correct for nonlinear behavior of stars over a substantial background count rate. This method requires measuring the flux of the point source in an appropriate aperture of radius r_n and consists of applying the flat field nonlinearity correction of Equation 2.5 to the average flux in that aperture. The appropriate radius to be used with the 512×512 format is $r_n = 5.5$ pixel, while for the 512z×1024 it is $r_n = 8.6$ pixel (applying the correction to the de-zoomed image).

In this Chapter we extend the above method to deal with more general non-uniform objects, in a way that was already suggested, but not tested by Greenfield. This method consists of smoothing the nonlinear image using a simple circular smoothing aperture having the radius r_n determined by Greenfield. The correction factor is then computed for each pixel of the smoothed image and finally the correction is applied to the corresponding pixel of the original image. We have tested this method using it to correct our severely nonlinear (maximum correction factor ~ 1.8) image of NGC 4552 obtained in 1993 with the F342W filter and comparing this photometric profile with that of the 1991 image, again corrected with the above algorithm (even though the nonlinearity does not exceed $\sim 5\%$). We have found that the two profiles agree to better than 2% over the whole intensity range.

The inverse of the above method will be used in this Chapter to simulate the effect of the FOC nonlinearity over a synthetic image of a galaxy, which will represent the "true" galaxy image. In this case one has to smooth the synthetic image, again using a circular smoothing aperture of radius r_n. The nonlinearity of each pixel is computed from the smoothed version of the synthetic image using Equation 2.5 and the nonlinearity is finally applied to original synthetic image.

As can be seen in Figure 2.2 this method of simulating the nonlinearity effect is able to reproduce very well (within 0.05 mag from $0.''1$ to $3''$ from the center of the galaxy) the sharp decrease of the 1993 F342W profile [panel (d)], compared to the 1991 F342W one [panel (g)]. In both cases the starting synthetic galaxy is exactly the same apart from a scaling factor.

Bibliography

Bender, R., Burstein, D., & Faber, S.M. 1992, ApJ, 399, 462

Bender, R., Burstein, D., & Faber, S.M. 1993, ApJ, 411, 153

Bender, R., Kormendy, J., & Dehnen, W. 1996, ApJ, 464, L123

Bolton, J.G., Savage, A., & Wright, A.E. 1979, Australian J. Phys. Suppl., 46, 1

Bertola, F., Cappellari, M., Burstein, D., Greggio, L., Renzini, A., di Serego Alighieri, S. 1995, Stellar Populations, ed. G. Gilmore & P. van der Kruit (Dordrecht: Kluwer), p. 445

Blandford, R.D., Netzer, H. & Woltjer, L. 1991, "Active Galactic Nuclei", Berlin: Springer Verlag

Brown, T.M., Ferguson, H.C., & Davidsen, A.F. 1995, ApJ, 454, L15

Brown, T.M., Ferguson, H.C., Davidsen, A.F., & Dorman, B. 1997, ApJ, 482, 685

Burstein, D., Bertola, F., Buson, L.M., Faber, S.M., & Lauer, T.R. 1988, ApJ, 328, 440

Cannizzo, J.K., Lee, H.M., & Goodman, J. 1990, ApJ, 351, 38

Cappellari, M., et al. 1998, in preparation

Carollo, C.M., Franx, M., Illingworth, G.D., & Forbes, D.A. 1997a, ApJ, 481, 710

Carollo, C.M., Danziger, I.J., Rich, R.M., & Chen, X. 1997b, ApJ, 491, 545

Ciotti, L., Pellegrini, S., Renzini, A., & D'Ercole, A. 1991, ApJ, 376, 380

Ciotti, L. & Ostriker, J.P. 1997, ApJ, 487, L105

Crane, P., Stiavelli, M., King, I.R., Deharveng, J.M., Albrecht, R., Barbieri, C., Blades, J.C., Boksenberg, A., et al. 1993, AJ, 106, 1371

Davies, R.L., Burstein, D., Dressler, A., Faber, S.M., Lynden-Bell, D., Terlevich, R.J., & Wegner, G. 1987, ApJS, 64, 581

Eracleous, M., Livio, M., Halpern, J.P., & Storchi-Bergmann, T. 1995, ApJ, 438, 610

Evans, C.R. & Kochanek, C.S. 1989, ApJ, 346, L13

Faber, S.M., Tremaine, S., Ajhar, E.A., Byun, Y.-I., Dressler, A., Gebhardt, K., Grillmair, C., Kormendy, J., et al. 1997, AJ, 114, 1771

Filippenko, A.V. & Sargent, W.L.W. 1989, ApJ, 342, L11

Filippenko, A.V., Ho, L.C., & Sargent, W.L.W. 1993, ApJ, 410, L75

Ford, H.C., Harms, R.J., Tsvetanov, Z.I., Hartig, G.F., Dressel, L.L., Kriss, G.A., Bohlin, R.C., Davidsen, A.F., et al. 1994, ApJ, 435, L27

Genzel, R., Hollenbach, D., & Townes, C.H. 1994, Rep. Prog. Phys., 57, 417

Greenfield, P. 1994, Instrument Science Report FOC-074

Hameury, J.-M., King, A.R., Lasota, J.-P., & Auvergne, M. 1994, A&A, 292, 404

Ho, L.C., Filippenko, A.V., & Sargent, W.L.W. 1995, ApJS, 98, 477

Ho, L.C., Filippenko, A.V., & Sargent, W.L.W. 1997, ApJS, 112, 315

Ho, L.C. 1998, in Observational Evidence for Black Hole in the Universe, ed. S.K. Chakrabati (Dodrecht: Kluver Academic Publishers), in press [astro-ph/9803307]

Holtzman, J.A., Burrows, C.J., Casertano, S., Hester, J.J., Trauger, J.T., Watson, A.M., & Worthey, G. 1995, PASP, 107, 1065

Jaffe, W., Ford, H., Ferrarese, L., Van Den Bosch, F., & O'Connell, R.W. 1996, ApJ, 460, 214

Jedrzejevski, R. 1992, Instrument Science Report FOC-028

Jenkins, C. R. 1982, MNRAS, 200, 705

Kochanek, C.S. 1994, ApJ, 422, 508

Kormendy, J. & Richstone, D. 1995, ARA&A, 33, 581

Kormendy, J., Bender, R., Magorrian, J., Tremaine, S., Gebhardt, K., Richstone, D., Dressler, A., Faber, S.M., et al. 1997, ApJ, 482, L139

Lauer, T.R., Ajhar, E.A., Byun, Y.-I., Dressler, A., Faber, S.M., Grillmair, C., Kormendy, J., Richstone, D., & Tremaine, S. 1995, AJ, 110, 2622

Loeb, A. & Ulmer, A. 1997, ApJ, 489, 573

Luminet, J.-P. & Barbuy, B. 1990, AJ, 99, 838

Macchetto, F., Pastoriza, M., Caon, N., Sparks, W.B., Giavalisco, M., Bender, R., & Capaccioli, M. 1996, A&AS, 120, 463

Magorrian, J., Tremaine, S., Richstone, D., Bender, R., Bower, G., Dressler, A., Faber, S.M., Gebhardt, K., et al. 1998, AJ, 115, 2285

Maoz, D., Filippenko, A.V., Ho, L.C., Macchetto, F.D., Rix, H.-W., & Schneider, D.P. 1996, ApJS, 107, 215

Miyoshi, M., Moran, J., Herrnstein, J., Greenhill, L., Nakai, N., Diamond, P., & Inoue, M. 1995, Nature, 373, 127

Nota, A., Jedrzejevski, R., Voit, M., Hack, W. 1996, FOC Instrument Handbook Version 7.0 (Baltimore: STScI)

Oke, J.B., Bertola, F., & Capaccioli, M. 1981, ApJ, 243, 453

Pellegrini, S. 1994, A&A, 292, 395

Press, H.P., Teukolsky, S.A., Wetterling, W.T., & Flannery, B.P. 1992, Numerical Recipes in FORTRAN 77, 2nd ed., Cambridge University Press, Cambridge

Rees, M.J. 1988, Nature, 333, 523

Rees, M.J. 1990, Science, 247, 817

Renzini, A. 1995, Fresh Views of Elliptical Galaxies, ed. A. Buzzoni, A. Renzini, & A. Serrano, PASP Conf. Ser. 86, 305

———. 1996, New Light on Galaxy Evolution, ed. R. Bender & R.L. Davies (Dordrecht: Kluwer), p. 131

Renzini, A., Greggio, L., Di Serego Alighieri, S., Cappellari, M., Burstein, D., & Bertola, F. 1995, Nature, 378, 39 (Paper I)

Schlegel, E.M., Petre, R., & Loewenstein, M. 1998, AJ, 115, 525

Storchi-Bergmann, T., Eracleous, M., Livio, M., Wilson, A.S., Filippenko, A.V., & Halpern, J.P. 1995, ApJ, 443, 617

Storchi-Bergmann, T., Eracleous, M., Ruiz, M.T., Livio, M., Wilson, A.S., & Filippenko, A.V. 1997, ApJ, 489, 87

Trinchieri, G. & Di Serego Alighieri, S. 1991, AJ, 101, 1647

Ulmer, A. 1997a, [astro-ph/9706247]

———. 1997b, [astro-ph/9708265]

Ulrich, M.-H., Maraschi, L., & Megan, C. 1997, ARA&A, 35, 445

Van Der Marel, R.P., De Zeeuw, P., Rix, H.-W., & Quinlan, G.D. 1997, Nature, 385, 610

Van Dokkum, P.G. & Franx, M. 1995, AJ, 110, 2027

Wrobel, J.M. 1991, AJ, 101, 127